JACS Au
AN OPEN ACCESS JOURNAL OF THE AMERICAN CHEMICAL SOCIETY

pubs.acs.org/jacsau
Article

Enhancing Cancer Vaccine Efficacy: Backbone Modification with β-Amino Acids Alters the Stability and Immunogenicity of MUC1-Derived Glycopeptide Formulations

Ruslan Gibadullin,* Óscar Suárez, Foivos S. Lazaris, Naiara Gutiez, Estibaliz Atondo, Sarai Araujo-Aris, Ander Eguskiza, Jiani Niu, Ariel J. Kuhn, Ana S. Grosso, Héctor Rodriguez, Fayna García-Martín, Filipa Marcelo, Tanausú Santos, Alberto Avenoza, Jesús H. Busto, Jesús M. Peregrina, Samuel H. Gellman, Juan Anguita,* Roberto Fiammengo,* and Francisco Corzana*

Cite This: JACS Au 2025, 5, 2270−2284

Read Online

ACCESS | Metrics & More | Article Recommendations | Supporting Information

ABSTRACT: Glycopeptides derived from the mucin-1 (MUC1) glycoprotein hold significant promise as cancer vaccine candidates, but their clinical utility is limited by proteolytic degradation and the poor bioavailability of L-α-amino acid−based peptides. In this study, we demonstrate that substitution of multiple α-amino acids with homologous β-amino acids (same side chain, but extended backbone) in *O*-glycosylated MUC1 derivatives significantly enhances their proteolytic stability. We further show that α-to-β substitutions within the most immunogenic epitope of MUC1 impede binding to an anti-MUC1 antibody, while substitutions outside the same epitope preserve antibody recognition. Structural investigations using circular dichroism, NMR spectroscopy, and molecular dynamics simulations reveal that the strongest α/β-peptide binders retain native-like conformations in the epitope region, both in their unbound state and when bound to the anti-MUC1 antibody. Conjugation of these high-affinity α/β-peptide analogs to gold nanoparticles induces robust immune responses in mice comparable to that of the native glycopeptide. Additionally, these α/β-analogs elicit elevated levels of the cytokine IFNγ, one of the key proteins for tumor cell elimination, surpassing levels produced by the native MUC1 glycopeptide. In contrast, a low-affinity α/β-analogue with lower proteolytic stability produces minimal cytokine responses, underscoring the critical role of these biochemical properties in vaccine efficacy. Collectively, our findings highlight that α-to-β modifications in the peptide backbone offer an effective strategy for developing biostable, highly immunogenic glycopeptide-based cancer vaccines, exemplifying the power of structure-based rational design in advancing next-generation vaccines.

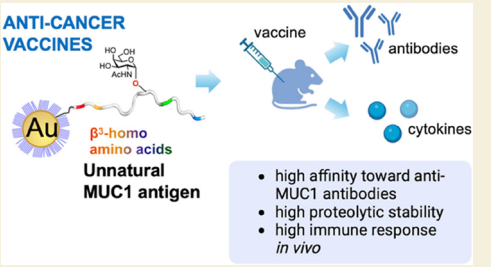

KEYWORDS: *mucin, glycopeptide, cancer vaccine, β-peptides, gold nanoparticles, proteolytic stability*

INTRODUCTION

Mucin-1 (MUC1) is a glycoprotein that is found on the surface of epithelial cells. The extracellular domain of MUC1 contains tandem repeats of 20-amino acid residues that are heavily *O*-glycosylated at five different S/T sites (potential glycosylated serine and threonine residues are shown in bold letters in Figure 1).[1,2] These *O*-glycosylation features allow MUC1 to play a key role in critical biological functions, such as cell protection, inflammation, and cell signaling. In cancer cells, however, glycosylated MUC1 residues display altered *O*-glycan profiles.[3−5] Instead of being decorated by branched and extended chains of glycans, these glycosylated residues bear only simple glycans, such as *N*-acetylgalactosamine (GalNAc). This substantial change in the glycosylation profile exposes different antigens within MUC1 that are otherwise hidden, such as the peptide fragment APDTRP (shown in pink in Figure 1) or tumor-associated carbohydrate antigens,[6−8] including the structurally simple Tn antigen (α-*O*-GalNAc-S/T or α-*O*-GalNAc-Ser/Thr).[9] Cancer patients have been shown to develop anti-MUC1 antibodies early in the disease,[10−12] likely in response to the exposure of antigens due to abnormal glycosylation patterns. Notably, the US National Cancer Institute ranked MUC1 as the number two prioritized antigen for the development of a cancer vaccine, underscoring the relevance of this glycoprotein as a tumor-associated antigen.[13]

Several vaccine candidates based on tumor-associated MUC1 (TA-MUC1) glycopeptides have been reported.[14−20] However, the results of these attempts in clinical trials remain mostly unsatisfactory.[1,21−23] In fact, there are two major

Received: February 27, 2025
Revised: May 7, 2025
Accepted: May 7, 2025
Published: May 15, 2025

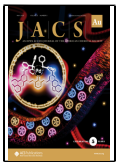

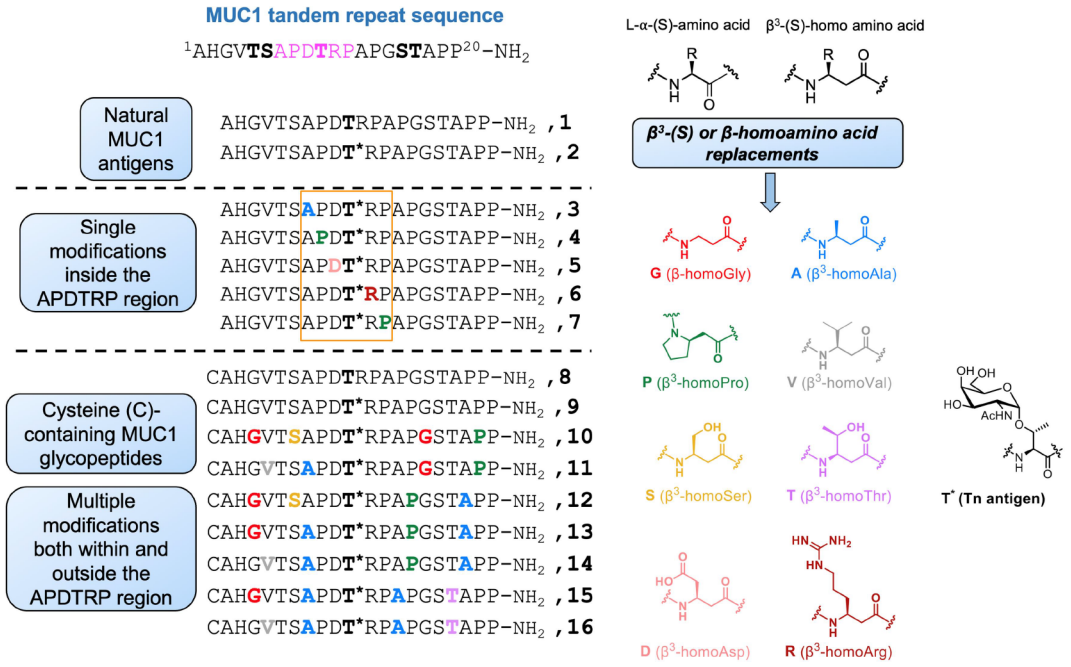

Figure 1. MUC1-derived glycopeptides studied in this work, featuring replacements of L-α-amino acid residues with homologous β^3-amino acids residues (side chain on the carbon adjacent to nitrogen) within the primary epitope (APDTRP) recognized by the SM3 antibody (**3**–**7**) or within and outside of this epitope (**8**–**16**). Each MUC1 derivative encompasses the tandem repeat sequence of the MUC1 glycoprotein, with the Tn antigen (T* = α-*O*-GalNAc-T) incorporated into the peptide sequence.

challenges for the clinical application of MUC1 vaccines. First, MUC1 glycopeptides are self-antigens, which means that they are generally tolerated by the immune system and fail to induce a robust immune response. Second, peptides composed of L-α-amino acid residues, including MUC1 glycopeptides, are prone to rapid proteolytic degradation in the blood or other biological fluids, which significantly reduces their bioavailability. Attempts to overcome these limitations include the use of artificial antigens containing unnatural residues with subtle chemical modifications[18,24−26] and the development of peptide analogs with unusual backbone subunits, such as those derived from D-α-amino acids,[27] peptoids (*N*-alkyl-glycine),[28,29] oligoureas,[30] thioamides,[31] or β-amino acids.[32−35] Such antigens are deemed to display greater immunogenicity with respect to the natural antigen, possibly evading tolerance while maintaining close enough structural homology to allow for immunological cross-reactivity. Additionally, such modifications can provide enhanced resistance against proteolysis.

Here, we evaluated the effect of replacing L-α-residues with homologous β-residues (same side chain but extended backbone; Figure 1) on the immunogenicity of MUC1-derived glycopeptide multivalently presented on the surface of gold nanoparticles (AuNPs). Although the impact of incorporating β-residues on recognition by the machinery of the immune system has been previously reported,[36] to our best knowledge, this type of backbone modification has not been previously evaluated for any TA-MUC1 glycopeptide. Arvidsson and coworkers[37,38] tested short glycopeptides composed entirely of β-amino acids for their ability to be recognized by plant lectins and, in many cases, the all-β-glycopeptides displayed a lower affinity for the lectin when compared to the all-α glycopeptide. Still, there were a few instances when the backbone modification increased the affinity of β-glycopeptides for the lectin.

We aimed to develop immunogenic formulations with unnatural MUC1 analogs containing β-amino acids that mimic the native antigen while enhancing their resistance against proteases. We were guided by previous efforts of the Gellman group involving periodic α-to-β replacements in various α-*helical* peptides, which showed that replacement of ∼30% of the residues can result in considerable resistance against proteolysis.[32,39−41] However, from the structural point of view, the impact of α-to-β replacements on the *extended* conformation of MUC1 glycopeptides in aqueous solution[24] is unknown.

In this work, we present the synthesis of several MUC1 glycopeptides with single or multiple α-to-β replacements and investigate their ability to bind to SM3, a murine monoclonal anti-MUC1 antibody,[42] used as a proxy protein for predicting immunogenicity in mice, as recently reported by us.[43] We also show that multiple α-to-β replacements conferred to the unnatural MUC1 glycopeptides enhanced their resistance against proteolysis. The two strongest SM3 binders, along with a different α/β-derivative that displays weaker SM3 affinity, were immobilized on the hydrophilic coating of gold nanoparticles (AuNPs)[44] and tested as vaccine candidates. Our results demonstrate that AuNP-MUC1 formulations were indeed immunogenic and generated antibodies that were cross-reactive toward the natural antigen found on two different human cancer cell lines. We then show that the AuNP-MUC1 formulations, which feature high-affinity glycopeptides for the SM3 antibody, elicited cellular immunity in mice, as evidenced by the release of IFNγ cytokine by isolated murine splenocytes after restimulation. Overall, our results highlight the benefit of the backbone modification approach for the development of vaccine candidates based on artificial MUC1 glycopeptides.

https://doi.org/10.1021/jacsau.5c00224
JACS Au 2025, 5, 2270−2284

RESULTS AND DISCUSSION

Design, Synthesis and Affinity of MUC1 α/β-Glycopeptides toward SM3 Antibody

We prepared peptides **1**-**7** by solid-phase peptide synthesis (SPPS; Figure 1). Peptides **1** and **2** represent nonglycosylated and glycosylated TA-MUC1 antigens, respectively, based on the 20-residue-long tandem repeat sequence of MUC1. Peptides **3**-**7** are glycosylated MUC1 analogs in which one L-α-residue has been replaced by a homologous β^3-residue (side chain on the carbon adjacent to nitrogen). The Fmoc-protected β^3-homoamino acids are commercially available, and they can be readily incorporated into peptides by SPPS. All glycopeptides contain the natural Tn antigen (T* = α-*O*-GalNAc-Thr) and were synthesized by stepwise microwave-assisted solid-phase synthesis with Rink Amide MBHA resin using the Fmoc strategy, as previously described.[44] Crude products were purified by RP-HPLC, lyophilized, and characterized (ESI).

For glycopeptides **3**−**7**, single α-to-β replacements were incorporated into the immunodominant sequence (APDTRP)[6−8] of the MUC1 glycopeptide. We investigated the affinity of these MUC1 variants for the SM3 antibody using a surface plasmon resonance (SPR) assay (Table 1, Figures S1−S4). SM3 is a well-characterized monoclonal antibody that was developed to recognize TA-MUC1.[42] SPR experiments were conducted at 25 °C using a Biacore X-100 system with a HBS-EP buffer (pH 7.5). The SM3 antibody was immobilized on a CM5 sensor chip via amine coupling, and glycopeptides were injected for affinity analysis, with data fitted to a two-site binding model by using Prism software. As expected, the SM3 antibody bound the glycosylated MUC1 peptide **2** with a 5-fold higher affinity compared to the nonglycosylated peptide **1** (Table 1; Figures S1 and S3), indicating that the GalNAc glycan *O*-linked to the side chain of threonine plays an additive role in the recognition of the MUC1 peptide backbone by SM3.[6,45] We observed a significant decrease in SM3 affinity among all α/β-glycopeptides **3**−**7** when compared to the natural glycopeptide **2** (Table 1; Figures S1 and S3). The strongest SM3 antibody binder in this set was glycopeptide **3** (α-to-β replacement at residue A7; ∼27-fold larger dissociation constant, K_D). Together, these results indicate that the SM3 antibody is highly sensitive to single α-to-β replacements within the APDTRP motif of the MUC1 glycopeptide.

Table 1. Binding Affinities (K_D) of Peptides 1−7 for the SM3 Antibody Were Determined with Surface Plasmon Resonance (SPR)

peptide	K_D (μM)[a]	K_D[b] relative
1	6.50 ± 0.73	5
2	1.30 ± 0.51	1
3	35 ± 5.9	27
4	910 ± 140	700
5	56 ± 2.6	43
6	1700 ± 130	1308
7	50 ± 3.6	38

[a]K_D (μM) values represent mean ± standard deviation from 3 independent assays. [b]Binding affinity normalized to peptide **2**.

Based on the data for single α-to-β replacements, we prepared additional α/β-glycopeptides **10**-**16** (Figure 1). These new analogs contained either four β^3 residues adjacent to the immunodominant region of the MUC1 tandem repeat peptide (APDTRP)[6] or three β^3 residues proximal to this region in addition to a β^3-homoalanine residue replacing alanine within the APDTRP region (Figure 1). New all-α controls, peptides **8** and **9**, were synthesized as well (Figure 1). Compared to the original peptides **1**−**7**, derivatives **8**-**16** were modified with an *N*-terminal cysteine residue that allowed for subsequent conjugation to gold nanoparticles (AuNPs). Our goal was to incorporate β^3 residues throughout the MUC1 sequence to provide significant protection from proteolysis; previous studies indicated that a portion of the α-residues, such as every third or fourth L-α-residue, can be replaced with a β-residue without disrupting the peptide's secondary structure.[32,39] The SPR assays (Table 2) demonstrated that the unnatural glycopeptides **10** and **12**, which retain the unaltered natural epitope APDTRP, exhibit affinities that are comparable to that of the all-α glycopeptide **9** (only ∼1.5- and 3-fold higher K_D, respectively; Table 2, Figures S2 and S4). Glycopeptide **13** was the next strongest SM3 binder (∼15-fold higher K_D relative to glycopeptide **9**); the decrease in SM3 affinity by glycopeptide **13** relative to the all-α glycopeptide **9** is likely due to the A7 modification within the critical APDTRP motif (Figure 1). The remaining four glycopeptides (**11** and **14**−**16**) showed significantly lower SM3 affinity (∼35−345-fold higher K_D relative to glycopeptide **9**); each of these analogs also contains an A7 modification within the APDTRP segment of MUC1.

Table 2. Binding Affinities (K_D) of Peptides 8−16 for the SM3 Antibody Were Determined with Surface Plasmon Resonance (SPR)

peptide	K_D (μM)[a]	K_D[b] relative
8	12 ± 1.3	11
9	1.10 ± 0.48	1
10	1.60 ± 0.28	1.5
11	60 ± 9.4	55
12	3.30 ± 0.29	3
13	17 ± 2.2	15
14	38 ± 8.4	35
15	270 ± 29	245
16	380 ± 82	345

[a]K_D (μM) values represent mean ± standard deviation from 3 independent assays. [b]Binding affinity normalized to peptide **9**.

Conformational Analysis of MUC1 α/β-Glycopeptides

To understand the favorable binding behavior of glycopeptides **10**, **12**, and **13** with the SM3 antibody at the molecular level, a detailed conformational analysis was carried out. This analysis included the evaluation of conformational states of the glycopeptide alone in solution and in the bound state with the SM3 antibody. Initial insights were gained by examining the circular dichroism (CD) spectra of these MUC1 α/β-analogs in comparison to their natural counterparts, **8** and **9** (Figure 2A). Each of the peptides exhibited a strong local minimum at 198 nm, which is representative of the random coil conformation.[46,47] These experiments revealed that the incorporation of four β^3-residues distributed within the MUC1 glycopeptide does not introduce any significant changes to the secondary structure of the glycopeptides alone in aqueous solution in comparison to the natural variants, **8** and **9**.

https://doi.org/10.1021/jacsau.5c00224
JACS Au 2025, 5, 2270−2284

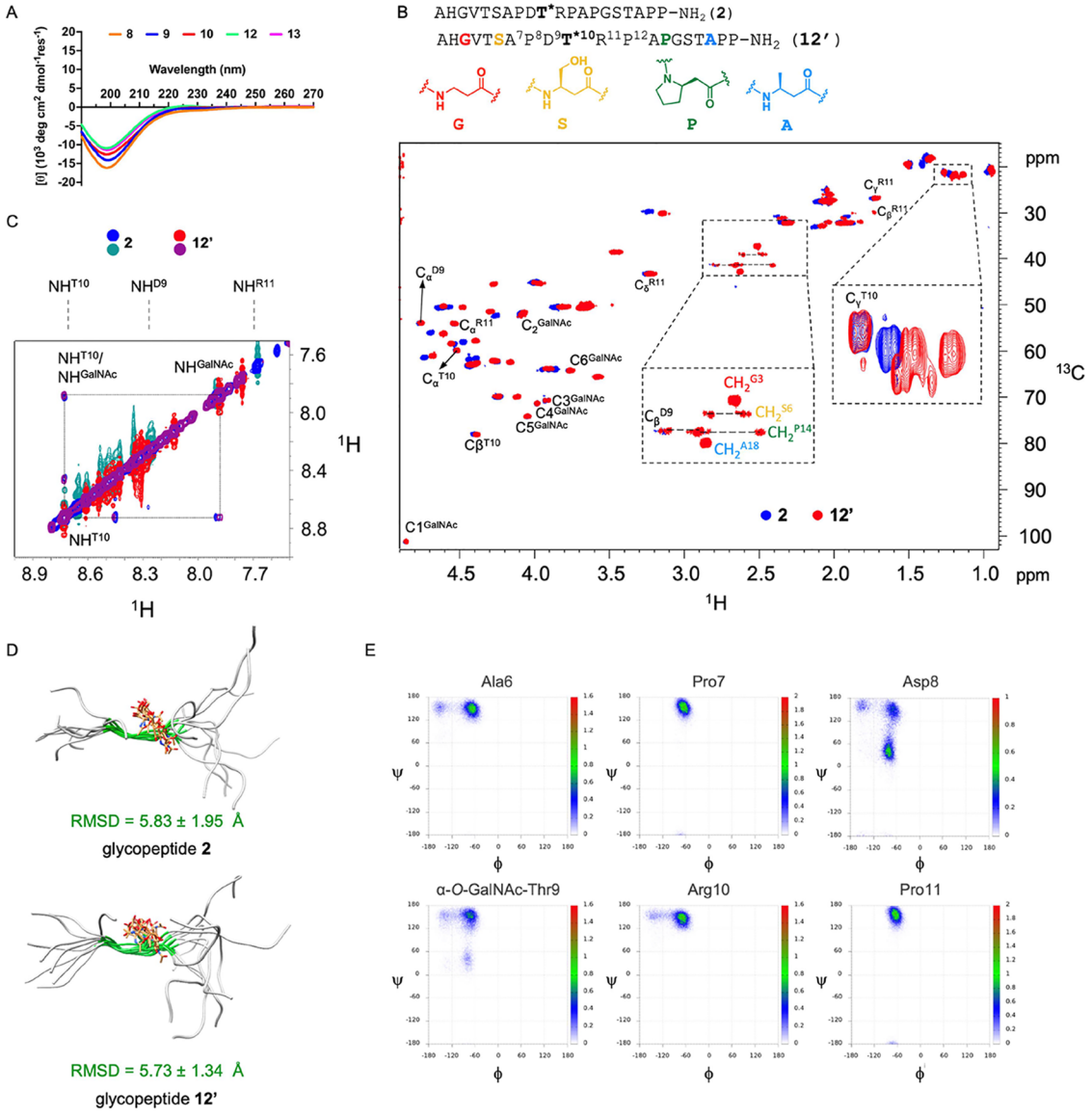

Figure 2. Conformational analysis of glycopeptides **2** and **12'** in water. (A) Near-UV circular dichroism data for MUC1 peptides (100 μM) measured in 10 mM phosphate buffer, pH 7.4. (B) Superimposition of the ^{1}H,^{13}C HSQC spectra for glycopeptides **2** (blue) and **12'** (red) acquired in a 10 mM phosphate buffer, pH 6.0, at 283 K at 500 MHz. The carbons belonging to the DTR region and GalNAc are marked. An expansion of the Cγ-Thr10 is highlighted by a gray dashed box. The labels of the CH_2 groups of the β-amino acid residues are also shown. (C) Superimposition of the NH region of the 2D NOESY spectrum (200 ms mixing time) of glycopeptides **2** (blue and green) and **12'** (red and purple). (D) Overlay of several frames of glycopeptides **2** and **12'** sampled from 300 ns experimental-guided MD simulations. RMSD values (±SD) of the APDTRP peptide backbone for both glycopeptides are shown. (E) φ/ψ distributions of the peptide backbone derived from 300 ns experimental-guided MD simulations for glycopeptide **12'**.

To obtain a more detailed understanding of conformational behaviors by MUC1 α/β-glycopeptides in water, we employed a synergistic approach involving NMR spectroscopy and molecular dynamics (MD) simulations. We performed these experiments using glycopeptide **12**, which displayed a very high affinity for the SM3 antibody using SPR (Table 2). We first analyzed the ^{1}H,^{13}C-HSQC spectrum of glycopeptide **12'** (a variant of glycopeptide **12** without the *N*-terminal Cys to prevent disulfide bridge formation; Figure 2B) in aqueous solution. For comparative purposes, we also conducted the same analysis on its natural variant, glycopeptide **2**. The superimposition of the Cα and Cβ atoms of the DTR residues in MUC1, observed in the ^{1}H,^{13}C-HSQC spectra, demonstrated a good match between glycopeptides **2** and **12'** (Figure 2B). Then, a detailed analysis of the 2D-NOESY spectra for these glycopeptides was conducted (Figure 2C). This analysis revealed strong NOE contacts between H$\alpha(i)$ and NH$(i + 1)$ for all residues in both glycopeptides, providing additional insights into their structural arrangements. As in previous studies, a distance between H$\alpha(i)$ and NH$(i + 1)$ of 2.1 ± 0.2 Å was used as a time-averaged restraint in experiment-guided MD simulations (Figure 2C,D). These simulations revealed that compounds **2** and **12'** exhibit unstructured peptide backbone conformations in solution (Figures 2D, E, and S6). However, an extended conformation is observed near the glycosylation site corresponding to the APDTRP epitope in both glycopeptides, with torsional angles (ϕ/ψ) for each residue in the APDTRP fragment approximating −80°/160°,

https://doi.org/10.1021/jacsau.5c00224
JACS Au 2025, 5, 2270−2284

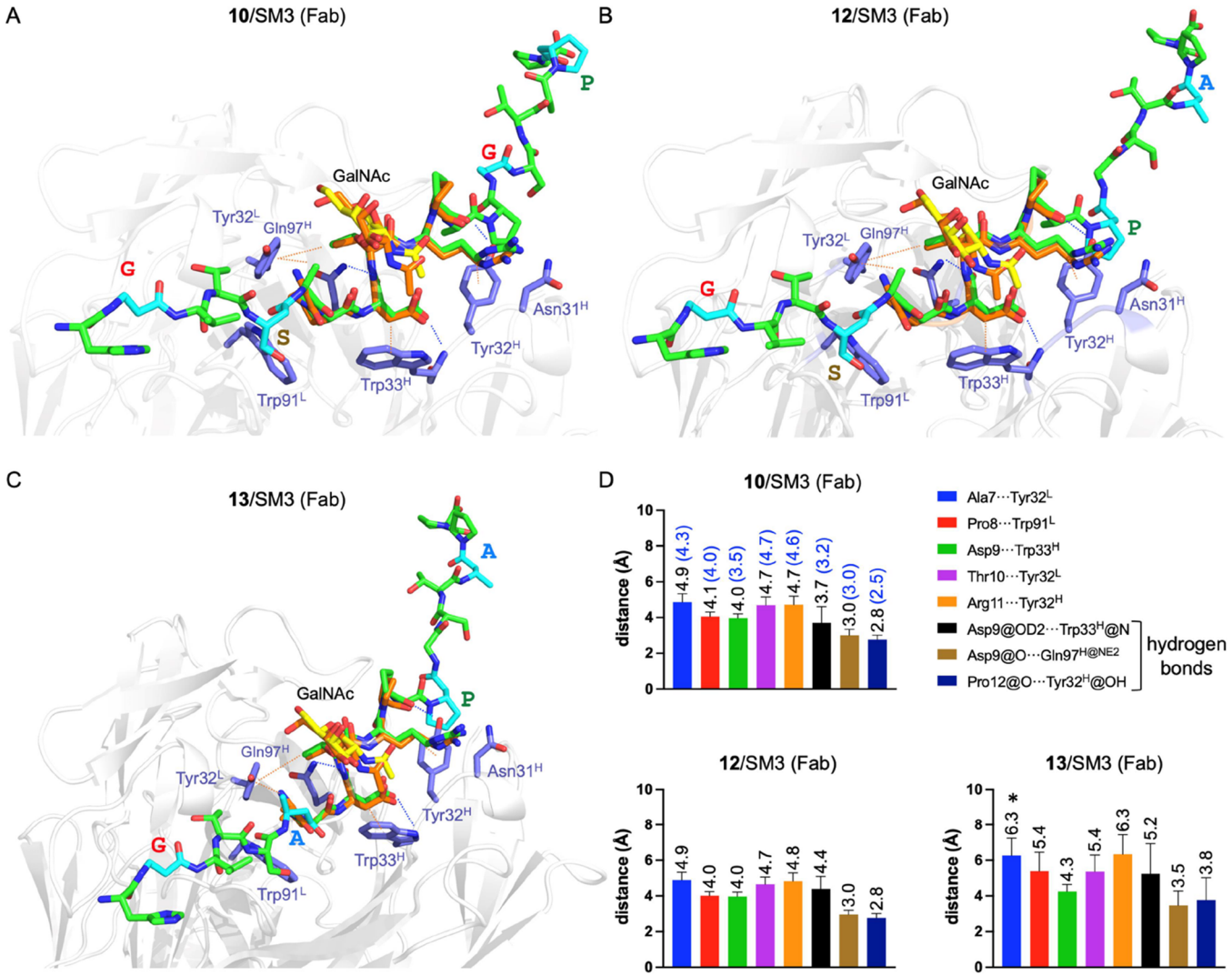

Figure 3. Structural characterization of MUC1 α/β-glycopeptides in complex with the SM3 antibody through MD simulations. Representative snapshots depicting the conformational arrangements of glycopeptides **10** (A), **12** (B), and **13** (C) bound to the Fab region of the SM3 antibody. The antibody is depicted as white ribbons, while the glycopeptides are depicted as sticks. The *N*-terminal Cys residue was removed in these calculations to facilitate a direct comparison with natural glycopeptide **2**. Unnatural β^3-residue carbon atoms are highlighted in blue, while GalNAc residues are shown in yellow. Antibody residues engaged in interactions with glycopeptides are shown as purple sticks. Hydrogen bonds and CH/π interactions are denoted by blue and orange dashed lines, respectively. The complexes are overlaid with the X-ray structure of the glycopeptide APDT*RP (in orange) in complex with scFV-SM3 (PD entry: 5A2K).[45] (D) Mean distance (±SD) between the atoms involved in hydrogen bonds and CH/π interactions across multiple complexes, computed from MD simulations. The center of mass of aromatic rings was used to calculate the distances involved in the CH/π interactions. The AMBER names were used for the atoms involved in the hydrogen bonds. The numbers in blue inside parentheses indicate the distances in the X-ray structure of a small glycopeptide containing the APDT*RP epitope in complex with SM3 (PDB entry: 5A2K).[45] See also Figure S8.

consistent with previous studies[48] (Figure 2D). This result suggests that the distal substitution of α-amino acids with β-amino acids does not disrupt the conformational behavior of this epitope and could explain the similar affinity of glycopeptides **2** and **12'** for the SM3 antibody. Additionally, both glycopeptides displayed the characteristic "eclipsed" conformer for the α-*O*-glycosidic linkage in which the threonine residue is involved,[49] with the sugar oriented perpendicularly to the peptide backbone (Figure S7). These findings suggest that the protease resistance observed for our unnaturally modified peptides (see the next section) is unlikely to arise from structural changes induced by the incorporation of β-amino acids. Instead, it is likely due to the chemical modification of the peptide backbone, which alters protease recognition, binding, and/or activity.

To study the binding interactions of glycopeptides **10**, **12**, and **13** with the SM3 antibody, we performed extensive molecular dynamics (MD) simulations. These simulations were initiated using coordinates derived from the crystal structure of the SM3 Fab fragment bound to a MUC1 peptide (PDB entry: 1SM3,[42] Figures 3 and S8). The stability of the glycopeptide-antibody complexes was confirmed throughout the MD trajectories. A previously reported X-ray structure[45] revealed that the all-α MUC1 glycopeptide (APDT*RP, where T* denotes the Tn antigen−α-*O*-GalNAc-Thr−) forms multiple hydrogen bonds and CH/π interactions with the SM3 antibody. Notable interactions include

https://doi.org/10.1021/jacsau.5c00224
JACS Au 2025, 5, 2270−2284

- CH/π interactions between Pro2, Asp3 and Arg5 side chains of the peptide and Trp91^{L}, Trp33^{H} and Tyr32^{H} of the antibody, respectively.
- Additional CH/π interactions involving Ala1 and Thr4 with Tyr32^{L}.
- Hydrogen bonds between the main chain of Thr4 and Gln97^{H}, and between the carboxylate moiety of Asp4 and Trp33^{H}.

The MD simulations of glycopeptides **10**, **12**, and **13** revealed that they maintain these key interactions (Figure 3A–C). However, significant differences were observed for glycopeptide **13**. The monitored distances for key interactions in this glycopeptide were greater than those for glycopeptides **10** and **12**. This increase in distance may explain the lower affinity of glycopeptide **13** for the SM3 antibody (Table 2). Notably, the substitution of the alanine residue 7 (A7) with a β^3-homoalanine residue in glycopeptide **13** allows for a CH/π interaction with Tyr32^{L}, though the slightly greater distance between the methyl group and the aromatic ring center impacts binding affinity.

Finally, to validate our approach, we also performed MD simulations for glycopeptide **6**, which exhibited a very low affinity for the SM3 antibody (K_D = 1700 μM; Table 1). In contrast to glycopeptides **10**, **12**, and **13**, compound **6** changed its binding mode during the simulations (Figure S8A). This shift prevented the formation of stabilizing contacts, such as hydrogen bonds and CH/π interactions, observed in the higher-affinity glycopeptides **9**, **10**, **12**, and **13**. The increased measured distances between interacting residues, as shown in Figure S8, further support this observation.

Proteolysis of MUC1 α/β-Glycopeptides

Incorporation of β-residues into peptides has been shown to hinder proteolysis.[32,39−41] We therefore analyzed the proteolytic stability of α/β-glycopeptides **10**, **12**, and **13** in the presence of proteinase K, a highly aggressive and promiscuous serine protease.[50] While MUC1 glycopeptides would not naturally encounter proteinase K in biological fluids, this protease provides a stringent test for the ability of α-to-β replacements to protect the MUC1 peptide against proteolysis due to its low substrate specificity (Figure 4A; eight cleavage sites were predicted for the MUC1 peptide). The PeptideCutter tool in Expasy predicts eight cleavage sites that are dispersed within all-α glycopeptide **9** (Figure 4A). Proteolysis reactions were monitored by UPLC, enabling the experimental determination of the half-life for each glycopeptide and clearly highlighting differences in degradation patterns among the compounds (Figures 4B and S5 and Table 3). Nonglycosylated and glycosylated all-α peptides **8** and **9** displayed comparable susceptibility toward cleavage by proteinase K, suggesting that the glycan on the side chain of T10 does not provide extra protection (1.5- and 1.1 min half-lives, respectively; Table 3).

Notably, two of the three α/β-glycopeptides, **10** and **12**, exhibited a considerable increase in stability, displaying ∼100-fold greater stability compared to that of the glycosylated MUC1 peptide **9** (Table 3). In contrast, α/β-glycopeptide **13** displayed a more moderate enhancement, with a ∼30-fold increase in peptide half-life against proteinase K relative to **9**.

Biological Analysis of MUC1 α/β-Glycopeptide AuNP-Conjugates

Our extensive structural analyses have so far demonstrated that the conformational behaviors of MUC1 α/β-glycopeptides **10** and **12** closely match the conformational behavior of their natural counterpart (**2**), both free in solution or when bound to the anti-MUC1 antibody, SM3. Therefore, based on this analysis and our recent findings with a different unnatural MUC1 analog,[43] we deemed MUC1 α/β-analogs **10** and **12** to be excellent candidates for vaccine formulation, vide infra. We also used analogue **13**, with lower affinity for the antibody SM3 (Table 2), for the preparation of a vaccine candidate. The *N*-terminal Cys residue present in these glycopeptides allowed conjugation to maleimide-functionalized PEGylated gold nanoparticles (AuNPs),[12,43,44] to provide conjugates AuNP-**10**, AuNP-**12**, and AuNP-**13** (Figures 5A and S9). A positive control (all-α glycopeptide **9**)[43] was conjugated to provide AuNP-**9**. It is important to note that the conjugation of these glycopeptides to AuNPs can further enhance their stability against enzymatic degradation.[51,52] The completion of conjugation reactions was confirmed by gel electrophoresis and dynamic light scattering analyses (Figure S10 and Table S1). All prepared AuNP-MUC1 conjugates were negatively charged, as indicated by their electrophoretic migration toward the cathode and confirmed by their negative ζ-potentials

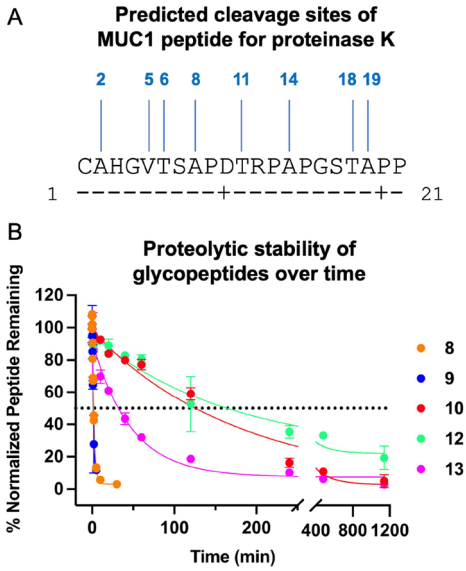

Figure 4. Proteolysis measurements for MUC1 peptides **8**, **9**, **10**, **12**, and **13**. (A) Predicted cleavage sites for MUC1 peptide against proteinase K obtained using the Expasy PeptideCutter tool. The cleavage occurs at the right site (*C*-terminal direction) of the amino acid marked with a vertical line. (B) Proteolysis time course curves of MUC1 glycopeptides in the presence of proteinase K, as monitored by UPLC. Uncertainties are expressed as the standard error of the mean (SEM). Normalized data were fit to a one-phase decay model and represent the average of 2 independent experiments (see Table 3).

Table 3. Proteolytic Stability of Selected MUC1 Peptides against Proteinase K

peptide	$t_{1/2}$ (min)[a]	$t_{1/2}$[b] relative
8	1.5	1.4
9	1.0	1.0
10	124	113
12	118	107
13	32	29

[a]$t_{1/2}$ (min) represent half-lives determined from one phase decay curves plotted using data obtained from two independent experiments. [b]Half-life normalized to glycopeptide **9**.

https://doi.org/10.1021/jacsau.5c00224
JACS Au 2025, 5, 2270−2284

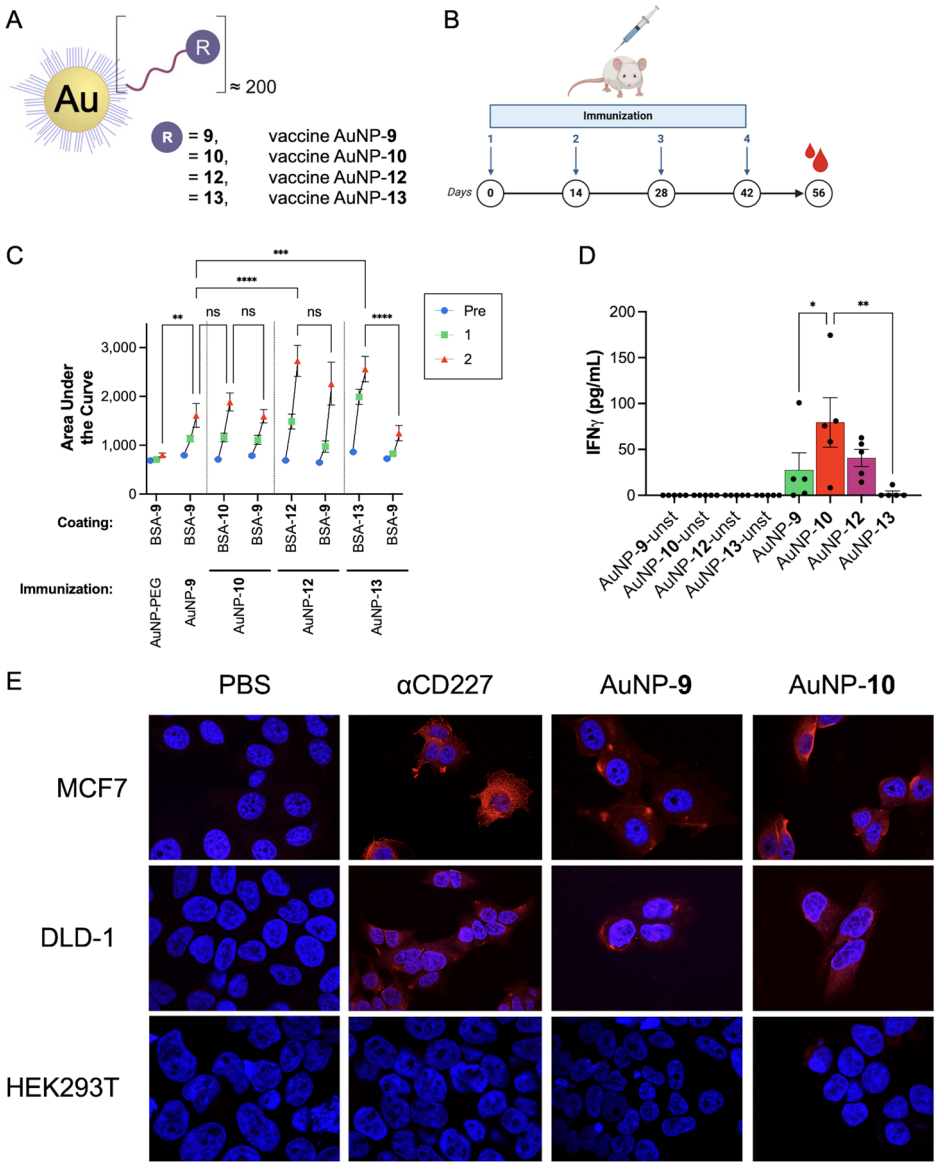

Figure 5. Schematic representation of vaccine candidates and in vivo studies. (A) Glycopeptides **9**, **10**, **12**, and **13** were conjugated to functionalized gold nanoparticles (AuNP-linker) via the *N*-terminal Cys residue. (B) Vaccine administration scheme used in this work. (C) Area under the curve (AUC) values for sera from different vaccine candidates measured using ELISA plates coated with either the natural or an unnatural BSA-conjugate. Statistical significance was calculated using a two-way ANOVA. $^{**}p < 0.01$; $^{***}p < 0.001$; $^{****}p < 0.0001$. Data represent mean + SD. (D) Th1 cytokine levels (IFNγ; $n = 5$), in mice treated with the different conjugates. Statistical significance was calculated using one-way ANOVA. $^{*}p < 0.05$; $^{**}p < 0.01$; $^{***}p < 0.001$). "Unst" stands for unstimulated cells (negative controls). (E) Confocal microscopy images show that mice antisera after vaccination with AuNP-**10** positively stain breast (MCF7) and colorectal adenocarcinoma (DLD-1) cancer cell lines that express tumor-associated MUC1, but not HEK293T cells, which lack MUC1 on their surface. The commercially available antibody αCD227 was used as a positive control for staining both the MCF7 and DLD-1 cancer cell lines.[53] Blue = Hoechst (nuclei); red = Alexa Fluor^{594}-labeled goat antimouse IgG. (B) was created using BioRender.

(Table S1). The number of antigen copies per AuNP was estimated by amino acid analysis, which suggested a loading of approximately 200 glycopeptides/AuNP.[44]

The four different AuNP-MUC1 conjugates (Figure 5A) formulated in phosphate-buffered saline (PBS) were used for a vaccination campaign, with each conjugate evaluated on a group of five BALB/c mice. AuNPs without any peptide conjugation (AuNP-PEG; Figure S9) were used as a negative control throughout these experiments. The animals were immunized with a prime dose followed by three equal booster doses (corresponding to 2 μg of glycopeptide for each formulation) at 14-day intervals. To analyze antibody production over time, murine blood was collected the day before the immunization (negative control) and 14 days after each injection. Mice were sacrificed 14 days after the last booster dose, and sera were collected (Figure 5B). Anti-MUC1 IgG antibodies were already detected after the first prime dose, and they reached their highest level after the first booster dose with either of the MUC1 conjugates (Figures 5C and S11); after this point, no further significant increase in the IgG antibody level was observed. Interestingly, the analysis of the total IgG levels showed that vaccine candidates with the unnatural glycopeptides (AuNP-**10**, -**12**, or -**13**) generated similar (AuNP-**10**) or superior (AuNP-**12**) antibody level

https://doi.org/10.1021/jacsau.5c00224
JACS Au 2025, 5, 2270−2284

compared to the formulation with the natural analogue AuNP-**9** (Figures 5C and S11); in contrast; AuNP-**13** elicited slightly lower IgG levels relative to AuNP-**9**. These experiments were carried out using an ELISA assay, in which plates were coated with bovine serum albumin (BSA) conjugates of either the natural or unnatural MUC1 glycopeptide for sera analysis (ESI and Figure S11).

Also of note is that cross-reactivity was detected among antibodies elicited by various MUC1 formulations. However, as an exception, the antibodies induced by AuNP-**13** were significantly more selective toward recognition of BSA-**13** than BSA-**9** (Figure 5C); this is likely because AuNP-**13** contains a backbone modification at the A7 residue of the critical APDTRP motif of MUC1 (Figure 1). In the remaining two cases where the A7 residue is unmodified, immunization with AuNP-**10** or AuNP-**12** elicited IgG antibodies with equal reactivity toward the used unnatural antigen (BSA-**10** or BSA-**12**) or the natural antigen, BSA-**9**.

The antisera of mice immunized with the AuNP-**10** conjugate were evaluated for their ability to stain human cancer cell lines displaying the tumor-associated MUC1 (TA-MUC1) on the cell surface. AuNP-**10** was chosen for these experiments because it demonstrated the strongest ability to enhance IFNγ cytokine production among the three unnatural MUC1 conjugates relative to AuNP-**9** (see below). We used MCF7[54] and DLD-1[55] cell lines, which are known for a high expression of TA-MUC1 on their cell surfaces; the MUC1-deficient HEK293T cell line[56] and PBS served as negative controls. Each of these cell lines was exposed to sera collected from mice immunized with AuNP-**9** or AuNP-**10**. Confocal microscopy experiments showed strong positive staining of TA-MUC1-expressing MCF7 and DLD-1 cell lines by the sera obtained from both AuNP-MUC1 formulations (Figure 5E). The commercially available anti-MUC1 antibody αCD227 was used as a positive control for staining both MCF7 and DLD-1 cancer cell lines.[53] As expected, we observed no staining of the TA-MUC1-lacking HEK293T cell line by sera collected from mice immunized with either of these MUC1 conjugates. A faint staining was observed when using AuNP-**10** sera on HEK293T cells, which is likely the result of cross-reactivity with antigens other than MUC1. This interpretation is supported by the lack of staining observed with the monoclonal anti-CD227 antibody.

We also assessed the production of the cytokine IFNγ by splenocytes isolated from C57BL/6 immunized mice after restimulation with individual AuNP-MUC1-conjugates (Figure 5D). The production of IFNγ serves as an indicator of the development of cellular immunity, including B cell help by $CD4^+$ T cells and cytotoxic $CD8^+$ T cell responses, which is particularly relevant for anticancer responses.[57] The vaccine candidate formulated with glycopeptide **10** (AuNP-**10**) induced the production of higher levels of IFNγ compared to those of the natural formulation (AuNP-**9**, Figure 5D). AuNP-**12** induced similar IFNγ levels compared to AuNP-**9**. Notably, vaccination with AuNP-**13**, featuring a single α-to-β replacement at A7 of the APDTRP region of MUC1, resulted in lower IFNγ levels, suggesting that the backbone modification at A7 likely precludes or leads to suboptimal presentation of the APDTRP motif by major histocompatibility complex I (MHC I) to $CD8^+$ T cells. Supporting this view, vaccination with the other three MUC1 conjugates (AuNP-**9**, **10**, or **12**), whose glycopeptides lack any modifications to their immunogenic APDTRP motif, generates higher levels of IFNγ (Figures 1 and 5D). These results are consistent with our past studies where we demonstrated that α-to-β replacements within MHC I peptides (i.e., MHCI/peptide complexes recognized by $CD8^+$ T cells) can modulate IFNγ cytokine levels in either direction.[33,36,58−61] Of note, none of the restimulation conditions produced detectable levels of IL-4 (data not shown), suggesting a strong bias toward a Th1-like response.

CONCLUSIONS

In this study, we have explored a novel strategy for modulating the efficacy of peptide-based cancer vaccine candidates: a backbone modification via homologous α-to-β replacements of a 20-residue glycopeptide derived from the MUC1 glycoprotein. Our original modification strategy focused on residues of the immunodominant sequence (APDTRP segment) of the variable number of tandem repeats domain of MUC1, a key region known to elicit B and T cell responses against MUC1 antigens.[22] However, we discovered that single α-to-β replacements within this segment of the peptide can dramatically decrease the binding affinity of the corresponding peptides (**3**-**7**) against anti-MUC1 antibody SM3 (Table 1). These results underscored the importance of the APDTRP backbone for recognition by the SM3 antibody and possibly other anti-MUC1 antibodies.[6,45]

Guided by these early results, we focused on introducing α-to-β replacements mainly outside of the APDTRP segment for all subsequent MUC1 analogs. This effort led to seven additional MUC1 analogs (**10**-**16**) containing four dispersed α-to-β replacements, with each modification positioned three or four residues apart from another to maximize protection against proteolysis and inflict minimal perturbation to the secondary structure of the glycopeptide.[32,39,41] In particular, two of these analogues (**10** and **12**) displayed a comparable binding affinity relative to that of the natural glycopeptide against the anti-MUC1 antibody (Table 2). Furthermore, analyses using CD and MD simulations demonstrated that glycopeptides **10** and **12** can adopt conformations that resemble those of the natural glycopeptide alone in aqueous solution or when bound to the Fab region of the anti-MUC1 antibody (Figures 2 and 3).

Interestingly, each of these three MUC1 α/β-analogs was less susceptible to proteolysis with proteinase K relative to the natural glycopeptide (Figure 4B and Table 3). These results are consistent with the known ability of β-residues to protect peptide bonds from proteolysis.[32,39−41,62,63] At this point, we concluded that MUC1 α/β-analogs **10** and **12** represent excellent vaccine candidates because the presence of multiple unnatural modifications should, in theory, increase the corresponding vaccine's immunogenicity and biostability. We, however, were unable to predict how these exact α-to-β replacements would modify MUC1 glycopeptide processing and loading onto MHCs or B cell receptors; a prediction of optimal peptide modifications and their processing patterns does not seem possible at this point for vaccine conjugates.

Gold nanoparticle (AuNP)-based vaccine formulations containing unnatural glycopeptides (AuNP-**10** and AuNP-**12**) elicited robust immune responses in mice, characterized by high IgG antibody levels in sera, comparable to the antibody levels generated using the natural antigen (AuNP-**9**; Figure 5C). More importantly, the antisera produced after vaccination with AuNP-**10** or AuNP-**12** were cross-reactive against natural antigen **9** at comparable reactivity (Figure 5C). In addition, the

https://doi.org/10.1021/jacsau.5c00224
JACS Au 2025, 5, 2270−2284

antisera from AuNP-**10** successfully stained two different TA-MUC1-positive cancer cell lines (Figure 5E). Additionally, we demonstrated that AuNP-**10** and AuNP-**12**, which display unnatural antigens with high affinity for SM3, could trigger cellular immunity to levels similar to that of AuNP-**9**, which displays the natural antigen (Table 2). This conclusion is supported by the detection of IFNγ levels upon splenocyte restimulation, which were comparable to or even higher after vaccination with unnatural antigens compared to natural antigens (Figure 5D). On the other hand, vaccine candidate AuNP-**13**, which carries antigen **13** possessing lower affinity for SM3 and shows reduced protection against proteolysis (Tables 2 and 3), elicited a weaker immune response and production of negligible levels of IFNγ when compared formulations with antigens **9**, **10**, and **12**.

From a vaccine design perspective, we acknowledge that direct comparisons between different immunization strategies are difficult due to the different animal models and experimental conditions used in various studies. However, under comparable experimental conditions, our results suggest a correlation between the strength of the immune response, as measured by antibody levels, and the in vitro binding affinity of the antigen to the SM3 antibody.

A key advantage of our gold nanoparticle (AuNP)-based approach is its ability to elicit a strong immune response without the need for an external adjuvant.[43,44] In contrast, carrier proteins such as KLH and CRM_{197} require an adjuvant to achieve high antibody levels.[26,64] Nonetheless, carrier proteins offer the benefit of presenting a limited number of antigens per conjugate. This was particularly evident in our CRM_{197} study,[26] where conjugation of a single antigen copy resulted in high antibody levels.

Overall, this study helps address two key challenges in peptide-based vaccines: immunological tolerance and the low bioavailability of the peptides. The beneficial properties of MUC1 α/β-analogs highlighted here, along with the commercial availability of many β-amino acids in Fmoc-protected form, should encourage further exploration of α/β-peptides and glycopeptides as promising antigen mimics.

METHODS

Solid-Phase Peptide Synthesis (SPPS)

(Glyco)peptides were synthesized by stepwise microwave-assisted solid-phase peptide synthesis on a Liberty Blue synthesizer using the Fmoc strategy on Rink Amide MBHA resin (0.1 mmol). Fmoc-Thr[GalNAc(Ac)$_3$-α-D]−OH was synthesized as described in the literature.[65] This Fmoc-protected glycosyl amino acid (2.0 equiv) was manually coupled using HBTU [(2-(1*H*-benzotriazol-1-yl)-1,1,3,3-tetramethyluronium hexafluorophosphate] (0.9 equiv) and diisopropyl ethyl amine (DIPEA, 2.0 equiv), while all other Fmoc amino acids (5.0 equiv) were automatically coupled using oxyma pure/DIC (*N*,*N*'-diisopropylcarbodiimide). *O*-acetyl groups of GalNAc moiety were removed by treating the resin-bound peptide with a mixture of NH_2NH_2 and MeOH (7:3), 3 × 5 mL. (Glyco)peptides were then released from the resin, along with removal of the acid-sensitive side chain protecting groups, using TFA 95%, triisopropylsilane (TIS) 2.5%, and H_2O 2.5% (3 mL) for 4 h at 25 °C. Glycopeptides containing an *N*-terminal Cys residue were treated with a solution of TFA/TIS/H_2O/EDT (92.5:2.5:2.5:2.5, 3 mL) for 4 h at 25 °C. (Glyco)peptides were then precipitated with cold diethyl ether (30 mL), and the mixture was centrifuged for 5 min at 3500 rpm. The supernatant solution was discarded, and this process was repeated once. Finally, (glyco)peptides were dried and redissolved in water to be purified by reverse-phase semipreparative RP-HPLC.

Surface Plasmon Resonance (SPR) Assays

SPR experiments were performed with a Biacore X-100 apparatus (Biacore, GE) in HBS-EP buffer at pH 7.5 (Hepes 10 mM, NaCl 150 mM, EDTA 3 mM, with 2% DMSO and 0.05% Tween X100) as the running buffer at 25 °C. The antibody SM3 (Abcam, ab22711) was immobilized on a CM5 sensor chip (Biacore, GE) following a standard amine coupling method. Briefly, the carboxymethyl dextran surface of flow-cell 2 was activated with a 7 min injection of a 1:1 ratio of aqueous 0.4 M 1-ethyl-3-(3-(dimethylamino)propyl) carbodiimide (EDC) and 0.1 M sulfo-*N*-hydroxysuccinimide. The antibody was coupled to the surface by adding 100 μg/mL protein solution diluted with 10 mM sodium acetate (pH 4.0) buffer using a flow rate of 10 μL/min for 7 min. The unreacted active esters on the surface were quenched by a 7 min injection of aqueous 0.1 M ethanolamine-HCl (pH 8.0). Flow cell 1, treated exactly like flow cell 2 but without the antibody, was used as a reference. Prior to use, 50 mM stock solutions of peptide ligand were diluted to the desired final concentration in running buffer. Typically, a series of different glycopeptides was injected onto the sensor chip at a flow rate of 30 μL/min for a period of 1 min, followed by a dissociation period of 1 min. No regeneration was needed. Sensorgram data were double referenced using the Biaevaluation X100 software (Biacore, GE). Three independent assays were performed for all evaluated glycopeptides. The experimental data of affinity measurements were fitted to a two-site-specific model binding using Prism software (Figures S1−S4).

Proteolysis Stability Studies

The PeptideCutter tool in Expasy predicts 8 cleavage sites that are dispersed within the Cys-residue containing natural glycopeptide **9** (Figure 4A, main text). For each proteolysis reaction, 20 μL of a 1 mM H_2O stock of peptide was diluted with 60 μL of DPBS, followed by the addition of 20 μL of proteinase K (25 μg/mL; freshly prepared in DPBS; Millipore Sigma, 70663−4). The final reaction solution contained 200 μM peptide and 5 μg/mL proteinase K. At each time point, a 10 μL aliquot of the reaction mixture was removed and immediately mixed with 20 μL of the quenching solution: 49.5% H_2O/49.5% MeCN/1% TFA. A "0 min" control was prepared by mixing 3 μL of a 1 mM H_2O stock of peptide with 12 μL of DPBS, after which 10 μL of this solution was removed and mixed with 20 μL of the quenching solution described above. A 10 μL aliquot of each quenched reaction solution was injected onto a Waters Acquity H-Class UPLC equipped with an Acquity BEH C18 column. 0% B hold over 1 min, followed by a 0−70% B gradient (A: Nanopure H_2O + 0.1% TFA; B: RP-HPLC-grade MeCN + 0.1% TFA) over the next 5 min, with a 0.3 mL/min flow rate was used for elution. The relative % of peptide remaining was quantified by integration of the peptide peak area at 220 nm and normalization to the "0 min" control (Figure S5). Each reaction was run in duplicate. Half-lives were determined by fitting normalized data to a one-phase decay model in GraphPad Prism 8.

Circular Dichroism (CD)

CD measurements of peptides were conducted at 25 °C on a JASCO J-1500 CD spectrometer. Peptides (100 μM) were dissolved in 10 mM phosphate buffer (pH 7.4), and the peptide solutions were then transferred to 1 mm quartz cuvettes. The CD spectrum was measured from 270 to 190 nm with 0.1 nm intervals and 4 s digital integration time at 100 nm/min scanning speed. CD data was averaged over 10 spectral scans. The data are presented as mean residue ellipticity in $deg{\cdot}cm^2{\cdot}dmol^{-1}{\cdot}res^{-1}$.

NMR Spectroscopy: Peptide Characterization

The glycopeptides (550−750 μM) were prepared in a buffer containing 10 mM sodium phosphate buffer (90:10, H_2O/D_2O) at pH 6.0. The ^{1}H NMR resonances of the glycopeptides were completely assigned through standard 2D-TOCSY (80 and 30 ms mixing time), and 2D NOESY (200 ms mixing time) experiments were acquired on a 600 MHz Bruker Avance III spectrometer equipped with a 5 mm inverse detection triple-resonance z-gradient cryogenic probe at 283 K. The ^{1}H,^{13}C HSQC spectra were acquired on a 500 MHz Bruker Ascend spectrometer equipped with a Prodigy

https://doi.org/10.1021/jacsau.5c00224
JACS Au 2025, 5, 2270−2284

cryoprobe CRPN2-TR-^{1}H&^{19}F/^{13}C/^{15}N-5 mm-EZ at 283 K. The resonance of 2,2,3,3-tetradeutero-3-trimethylsilylpropionic acid (TSP) was used as a chemical shift reference in the ^{1}H NMR experiments (δ TSP = 0 ppm). All spectra were processed and calibrated with TopSpin 4.4.0. The assignments were done using the software CARA (Computer Aided Resonance Assignment)[66] version 1.9.1.7.

Molecular Dynamics (MD) Simulations of Glycopeptides 6, 10, 12, and 13 in Complex with the SM3

The simulations were carried out with the AMBER 20 package[67] implemented with ff14SB,[68] GAFF,[69] and GLYCAM06j[70] force fields. The parameters and charges for the unnatural amino acids were generated with the antechamber module of AMBER, using the GAFF force field and the AM1-BCC method[71] for charges. The *N*-terminal Cys residue was removed in these calculations to facilitate a direct comparison with natural glycopeptide **2**. The crystal structure of the Fab structure of SM3 in complex with a peptide (PDB entry: 1SM3)[42] was used in these studies. Each molecule was then immersed in a water box with a 10 Å buffer of TIP3P water molecules.[72] The system was neutralized by adding explicit counterions. A two-stage geometry optimization approach was performed. The first stage minimizes only the positions of solvent molecules, and the second stage is an unrestrained minimization of all of the atoms in the simulation cell. The systems were then gently heated by incrementing the temperature from 0 to 300 K under a constant pressure of 1 atm and periodic boundary conditions. Harmonic restraints of 30 kcal·mol^{-1} were applied to the solute, and the Andersen temperature-coupling scheme was used to control and equalize the temperature. The time step was kept at 1 fs during the heating stages, allowing potential inhomogeneities to self-adjust. Long-range electrostatic effects were modeled using the particle-mesh-Ewald method.[73] An 8 Å cutoff was applied to Lennard-Jones interactions. Each system was equilibrated for 2 ns with a 2 fs time step at a constant volume and temperature of 300 K. Production trajectories were then run for an additional 1.0 μs under the same simulation conditions (Figures 3, main text, and S8).

Preparation and Characterization of Gold Nanoparticles (AuNPs)

All glassware employed for nanoparticle preparation was cleaned with aqua regia and HCl (37%)/HNO_3 (65%) 3:1. Ultrapure deionized water (Milli-Q Advantage A10 Water Purification System, 18.2 MΩ cm) was used for the preparation of all aqueous solutions. All solutions used for nanoparticle preparation were filtered through 0.22 μm membrane filters (cellulose acetate, Whatman Puradisc 30/0.2 or Corning cat. # 430513). AuNPs were characterized by Dynamic Light Scattering (DLS) (Litesizer DLS 500, Anton Paar). AuNP core diameter was measured via TEM (JEOL JEM-1011 transmission electron microscope operating at an accelerating voltage of 100 kV). UV/vis measurements were carried out using a TECAN Infinite M200 Pro plate reader. The concentration of AuNPs was determined by measuring the absorbance at 526 nm of samples dispersed in water in comparison with AuNP samples whose concentration was independently quantified via inductively coupled plasma-optical emission spectrometry (ICP-OES), assuming the nanoparticles were spherical. Citrate-coated AuNPs with a diameter of 13.0 ± 1.0 nm were synthesized according to a literature procedure.[74] AuNPs were passivated by the formation of self-assembled monolayers of alkyl-PEG600 thiols on their surface. We used mixtures of carboxy- and amino-terminated PEG600-thiols, with the molar fraction of amino-terminated derivative being x_{NH_2}= 0.20 (Figure S8). Stock solutions of thiols in EtOH (5 mM) were freshly prepared and directly used. Final concentrations in the passivation reaction were: ∼100 nM AuNPs, 25 mM $NaHCO_3$, 1 mM thiols (total), and therefore the reaction contained 20% v/v of EtOH. Stirring at room temperature was continued for 96 h, after which AuNP-PEG was purified by ultrafiltration in 100 kDa Amicon Ultra-15 centrifugal filters (1 × 15 mL 25 mM $NaHCO_3$, 1 × 15 mL 2:8 v/v EtOH/50 mM $NaHCO_3$, and 2 × 15 mL 50 mM $NaHCO_3$ buffer). Once purified, AuNP-PEG was taken up in H_2O at a final concentration varying in the interval 400−600 nM (Figure S9). Glycopeptides **9**, **10**, **12**, and **13** were coupled to AuNP-PEG according to a previously reported procedure, with minor modifications.[43] Shortly, AuNP-PEG were resuspended in 30 mM phosphate buffer at pH 8.2 (approximately 100 nM) and reacted with $SM(PEG)_2$ linker (cat. nr. 22102 Thermo Scientific, 5 mM in the reaction mixture). The reaction mixture was shaken for 4 h at 1 °C and 500 rpm. AuNP-Linker was then purified from excess linker via ultrafiltration in 100 kDa Amicon Ultra-4 centrifugal filters (1 × 4 mL H_2O, 1 × 4 mL 2:8 EtOH/20 mM phosphate buffer pH 8.2, and 2 × 4 mL H_2O) while performing all steps on ice, in a 4 °C-cooled centrifuge, and using ice-cold wash solutions. Purified AuNP-linker was taken up in water at a concentration of approximately 400 nM. In parallel, 200 μL of 500 μM glycopeptide solutions in H_2O were incubated with 10 mM tris(2-carboxyethyl)phosphine hydrochloride (TCEP) for 2 h at 0 °C to reduce any possible symmetric disulfide formation. For the coupling reactions, the necessary amount of freshly TCEP-treated glycopeptide was added to a freshly prepared cold solution of AuNP-linker and shaken overnight at 4 °C, 500 rpm. Typical conditions for the coupling reactions were: volume 600 μL, AuNP-linker ∼140 nM, 15 mM phosphate buffer pH 7.0, 50 μM glycopeptide (final concentrations in the reaction mixture). Excess of the uncoupled glycopeptide and TCEP was removed by centrifugation (20,800×*g*, 45 min, 18 °C), removal of the supernatant, and resuspension in 25 mM $NaHCO_3$ (2×) followed by purification using Vivaspin Turbo 4 Ultrafiltration Units (washing with 1 × 4 mL 10 mM $NaHCO_3$, 2 × 4 mL 2:8 v/v EtOH/10 mM $NaHCO_3$ and 1 × 4 mL 10 mM $NaHCO_3$). AuNPs were then taken up in 10 mM $NaHCO_3$ and further purified by gel filtration on NAP-10 columns preconditioned with 10 mM $NaHCO_3$. AuNP eluates were concentrated by centrifugation to approximately 500 μL and sterile filtered using Costar Spin-X Centrifuge Tube Filters with 0.22 μm cellulose acetate porous membranes. The filtered solutions (approximately 100 nM) were added to 10x phosphate-buffered saline (PBS) and diluted with sterile Milli-Q water to afford the final AuNP formulations used for mice vaccination (45 nM AuNPs in 1 × PBS).

Gel Electrophoresis

Gel electrophoresis was carried out on a 0.6% agarose gel using sodium boric acid (SB) buffer pH 8.5, for approximately 2 h at 60 V (Figure S10).[75] Nanoparticle samples were diluted with a loading buffer (1:1 SB buffer/glycerol) to 25 nM AuNPs before being loaded on the gel (∼10 μL/lane).

Dynamic Light Scattering (DLS) and Zeta-Potential Measurements

The mean z-average diameter and the PDI of the AuNPs were determined by dynamic light scattering via cumulant analysis of the time autocorrelation function. AuNPs were suspended in 10 mM $NaHCO_3$. Zeta potentials were measured using the same conditions (Table S1).

Preparation of Glycopeptide BSA Conjugates for ELISA Plate Coating

Bovine serum albumin (BSA, A0281 Sigma-Aldrich) was first derivatized using the $SM(PEG)_2$ amine-to-sulfhydryl heterobifunctional linker, followed by conjugation of glycopeptides **9**, **10**, **12**, and **13**. Shortly, $SM(PEG)_2$ (5×10^{-3} mmol in 100 μL dry acetonitrile, final conc. Five mM in the reaction mixture) was added to an aqueous solution of BSA in phosphate buffer at pH 8.2 (final reaction volume 1.0 mL, BSA 30 μM, buffer 30 mM). The reaction mixture was incubated at 1 °C for 3 h. Excess linker was then removed by ultrafiltration on Microcon-30 kDa Centrifugal Filter Unit with Ultracel30 membrane (washing with 3 × 500 μL 20 mM phosphate buffer pH 7.0). All cleaning steps were performed on ice, in a 4 °C centrifuge, and with ice-cold wash solutions. Purified linker-functionalized BSA was taken up in 1.0 mL of 20 mM phosphate buffer, pH 7.0, at a concentration of 1.4 mg/mL (∼21 μM). In parallel, 400 μL of 500 μM of the corresponding glycopeptide in water was incubated with 250 μM tris(2-carboxyethyl)phosphine hydrochloride (TCEP)

https://doi.org/10.1021/jacsau.5c00224
JACS Au 2025, 5, 2270−2284

for 1 h at rt to fully reduce any possible symmetric disulfide. For the peptide coupling reaction, 325 μL of freshly TCEP-treated glycopeptide was added to the freshly prepared cold solution of linker-functionalized BSA (480 μL, 21 μM) and shaken at 500 rpm overnight at 4 °C. The typical reaction volume was 1500 μL, and the final concentrations in the reaction mixture were: linker-functionalized BSA ∼6.7 μM, 30 mM phosphate buffer pH 7.0, 108 μM peptide. Excess uncoupled peptide was removed by ultrafiltration on Amicon Ultra-4 Centrifugal Filter Units, regenerated cellulose − 30 kDa (3 × 4 mL PBS). Purified conjugates were taken up in 500 μL of PBS at a concentration of 1.2 mg/mL (∼18 μM). The sample was stored protected from light at +4 °C and used to coat the ELISA plates for the determination of antigen-specific antibody titers (Figure S10).

In Vivo Studies

Animal experiments were conducted at the Animal Facility of CIC bioGUNE, an AAALAC Intl.-accredited facility. Animal work was performed in accordance with Spanish and European regulations and followed FELASA guidelines and recommendations concerning laboratory animal welfare. All animal experiments were approved by the Competent Authority (Diputación de Bizkaia) and the authorized Animal Ethics Committee (CIC bioGUNE's Committee of Animal Welfare and Biosafety, CBBA). Balb/c (BALB/cAnNCrl) andC57Bl/6 (C57BL/6J) mice (8 weeks old) were purchased from Charles River (Spain). Animals were maintained under 12 h light/dark cycles while receiving food and water ad libitum. In the experiments, we conducted the experiments with Balb/c mice. Mice, in groups of five, received subcutaneous injections of AuNP-**9**, AuNP-**10**, AuNP-**12**, or AuNP-**13** at 14-day intervals. Each injection contained 2 μg of the corresponding peptide. AuNPs without any peptide conjugation (**AuNP-PEG**, Figure S9) were used as a negative control. To analyze antibody production over time, murine blood was collected by submandibular puncture the day before the immunization and 14 days after each injection, and by cardiac puncture at sacrifice. Blood was collected in BD Microtainer tubes with serum separator gel, centrifuged at 10,000x rpm for 10 min, and the sera were stored at −80 °C until further use. At sacrifice, spleens were also collected in PBS and kept at 4 °C until splenocyte isolation. We found that the antibody titers did not change after the second, third, or fourth immunization (Figure S11).

Antibody Titer Determination by Enzyme-Linked Immunosorbent Assay (ELISA)

Antibody production was measured by an indirect enzyme-linked immunosorbent assay (ELISA). NUNC plates (Thermo Fisher) were coated at 4 °C overnight in 0.2 M sodium carbonate at pH 9.6, containing 0.2 μg/mL of BSA-conjugated glycopeptide **9**, **10**, **12**, or **13** or unconjugated BSA. Following four washes with 0.05% Tween-PBS (PBST), plates were blocked for 1 h with filtered 1% BSA-PBST. After aspiration, 2-fold serial dilutions of the sera, starting at 1/100, were applied and incubated for 1 h at room temperature. After six washes with PBST, the plates were incubated for 45 min with a goat antimouse total IgG antibody conjugated to horseradish peroxidase (HRP) (Jackson ImmunoResearch), diluted 1/5.000 in PBST. The plates were washed eight times with PBST and twice with PBS. 100 μL of 3,3′,5,5′-tetramethylbenzidine peroxidase substrate solution (TMB, SeraCare) was added to each well and incubated for 30 min. After the reaction was stopped with 100 mL of 1 M sulfuric acid solution, the absorbance at 450 nm of each sample was measured with a BioTek Epoch Microplate Spectrophotometer.

Splenic T-Cell Stimulation

The spleens from the immunized mice were disrupted using a 5 mL syringe plunge and filtered through a 70 μm pore cell strainer (Corning). Cells were collected in Dulbecco's Modified Eagle Medium (DMEM, Gibco) and centrifuged at 300×*g* for 5 min at 4 °C. The cells were resuspended in ammonium chloride potassium (ACK) lysis buffer and incubated for 5 min at room temperature. Red blood cell lysis was stopped by adding 2 volumes of 1x PBS. The cell solution was then pelleted by centrifugation at 300 g for 5 min at 4 °C and resuspended in 1%FBS-PBS. Automatic cell counting was performed using a 0.4% solution of trypan blue (Invitrogen) in a Countess II Automated Cell Counter (Invitrogen). The cells were finally resuspended in TexMACS medium (Miltenyi Biotec) supplemented with a 1% penicillin/streptomycin antibiotic solution (P/S, Gibco). The cells were seeded in 48-well plates (2×10^7 cells/well) and restimulated with 10 μg/mL of each peptide. A solution of PBS was used as the negative control. As a positive control, splenocytes were incubated with 100 ng/mL PMA and 125 ng/mL of ionomycin. The restimulation supernatants were recovered after 48 h and analyzed for IFNγ levels by capture ELISA using the BD OptEIA Mouse IFNγ ELISA Set (BD Biosciences), following the manufacturer's instructions.

Antibody Reactivity toward MUC1 Positive Cancer Cells Analyzed by Confocal Microscopy

MCF7 and DLD1 tumor cells were cultured in DMEM and Roswell Park Memorial Institute (RPMI) 1640 medium (Gibco), respectively, supplemented with 10% FBS (Gibco) and 1% P/S. HEK293T cells were used as a negative control and cultured using DMEM supplemented with 10% FBS and 1% P/S. For microscopy assays, MCF7 and DLD1 cells were collected by trypsinization (0.05% Trypsin-EDTA, Gibco), seeded on top of sterile round cover glasses in 24-well plates (2×10^5 cells/well), and allowed to adhere overnight. HEK293T cells were collected by pipetting and seeded on top of sterile round cover glasses pretreated with poly-L-lysine for 5 min and then extensively washed with MiliQ water and dried overnight at room temperature. After washing with 1x PBS, the cells were fixed with 4% paraformaldehyde in PBS for 20 min at 4 °C. After three washes, cells were incubated with 10% FBS-PBS blocking buffer for 1 h at 37 °C and then 2 h at 4 °C with antisera of immunized mice at a 1/100 dilution in blocking buffer, a CD227 monoclonal antibody (clone VU-3C6, Bio-Rad, 1/500) or blocking buffer (control). The cells were washed three times and then incubated for 2 h at 4 °C in the dark with AlexaFluor^{594}-labeled goat antimouse IgG secondary antibody (Invitrogen, 1/1000). After three washes, cell nuclei were stained with 0.2 μg/mL DAPI (Invitrogen) for 10 min at 4 °C. Glass coverslips were then mounted onto a microscope slide containing ProLongTM Gold Antifade Mounting reagent (Invitrogen). The preparations were analyzed by using a TCS SP8 confocal system (Leica Microsystems). Image analysis was performed by using the Leica Application Suite X software (version 3.7).

■ ASSOCIATED CONTENT

Supporting Information

The Supporting Information is available free of charge at https://pubs.acs.org/doi/10.1021/jacsau.5c00224.

Synthesis and characterization of the (glyco)peptides studied in this work, SPR assays, proteolysis stability studies, circular dichroism studies, ^{1}H,^{13}C-HSQC and 2D-NOESY, MD simulations, preparation and characterization of gold nanoparticles, and in vivo studies (PDF)

■ AUTHOR INFORMATION

Corresponding Authors

Ruslan Gibadullin − *Department of Chemistry, University of Wisconsin, Madison, Wisconsin 53706, United States;* Present Address: Department of Chemistry, The Scripps Research Institute, La Jolla, California 92037, United States; orcid.org/0000-0001-8439-0218; Email: rgibadullin@scripps.edu

Juan Anguita − *Inflammation and Macrophage Plasticity Laboratory, CIC BioGUNE, BRTA, 48160 Derio, Spain; Ikerbasque, Basque Foundation for Science, 48009 Bilbao, Spain*; Email: janguita@cicbiogune.es

Roberto Fiammengo − *Department of Biotechnology, University of Verona, 37134 Verona, Italy;* orcid.org/0000-0002-6087-6851; Email: roberto.fiammengo@univr.it

Francisco Corzana − *Departamento de Química and Instituto de Investigación en Química de la Universidad de La Rioja (IQUR), Universidad de La Rioja, 26006 Logroño, Spain;* orcid.org/0000-0001-5597-8127; Email: francisco.corzana@unirioja.es

Authors

Óscar Suárez − *Departamento de Química and Instituto de Investigación en Química de la Universidad de La Rioja (IQUR), Universidad de La Rioja, 26006 Logroño, Spain*

Foivos S. Lazaris − *Departamento de Química and Instituto de Investigación en Química de la Universidad de La Rioja (IQUR), Universidad de La Rioja, 26006 Logroño, Spain;* orcid.org/0000-0003-4292-8723

Naiara Gutiez − *Inflammation and Macrophage Plasticity Laboratory, CIC BioGUNE, BRTA, 48160 Derio, Spain*

Estibaliz Atondo − *Inflammation and Macrophage Plasticity Laboratory, CIC BioGUNE, BRTA, 48160 Derio, Spain*

Sarai Araujo-Aris − *Inflammation and Macrophage Plasticity Laboratory, CIC BioGUNE, BRTA, 48160 Derio, Spain*

Ander Eguskiza − *Department of Biotechnology, University of Verona, 37134 Verona, Italy*

Jiani Niu − *Department of Chemistry, University of Wisconsin, Madison, Wisconsin 53706, United States;* orcid.org/0000-0002-5090-5516

Ariel J. Kuhn − *Department of Chemistry, University of Wisconsin, Madison, Wisconsin 53706, United States*

Ana S. Grosso − *UCIBIO - Applied Molecular Biosciences Unit, Department of Chemistry and Associate Laboratory i4HB - Institute for Health and Bioeconomy, NOVA School of Science and Technology, 2829-516 Caparica, Portugal*

Héctor Rodriguez − *Inflammation and Macrophage Plasticity Laboratory, CIC BioGUNE, BRTA, 48160 Derio, Spain*

Fayna García-Martín − *Departamento de Química and Instituto de Investigación en Química de la Universidad de La Rioja (IQUR), Universidad de La Rioja, 26006 Logroño, Spain*

Filipa Marcelo − *UCIBIO - Applied Molecular Biosciences Unit, Department of Chemistry and Associate Laboratory i4HB - Institute for Health and Bioeconomy, NOVA School of Science and Technology, 2829-516 Caparica, Portugal*

Tanausú Santos − *Departamento de Química and Instituto de Investigación en Química de la Universidad de La Rioja (IQUR), Universidad de La Rioja, 26006 Logroño, Spain*

Alberto Avenoza − *Departamento de Química and Instituto de Investigación en Química de la Universidad de La Rioja (IQUR), Universidad de La Rioja, 26006 Logroño, Spain;* orcid.org/0000-0002-5465-3555

Jesús H. Busto − *Departamento de Química and Instituto de Investigación en Química de la Universidad de La Rioja (IQUR), Universidad de La Rioja, 26006 Logroño, Spain;* orcid.org/0000-0003-4403-4790

Jesús M. Peregrina − *Departamento de Química and Instituto de Investigación en Química de la Universidad de La Rioja (IQUR), Universidad de La Rioja, 26006 Logroño, Spain;* orcid.org/0000-0003-3778-7065

Samuel H. Gellman − *Department of Chemistry, University of Wisconsin, Madison, Wisconsin 53706, United States;* orcid.org/0000-0001-5617-0058

Complete contact information is available at: https://pubs.acs.org/10.1021/jacsau.5c00224

Author Contributions

R.G., O.S., F.G.M., J.M.P., S.H.G., and F.C. performed the synthesis, purification, and characterization of the glycopeptides. F.S.L., A.E., and R.F. conducted the synthesis of the AuNPs, their conjugation to glycopeptides, and full characterization of the nanomaterials. N.G., E.A., S.A.-A., H.R., and J.A. carried out in vitro and in vivo studies, analyzed antibody levels, cytokine (IFNγ) production, and conducted confocal microscopy experiments. A.S.G., J.M.P. and F.M. performed NMR experiments and conformational analysis of the glycopeptides by NMR. J.N., A.J.K., and R.G. conducted circular dichroism studies and proteolysis measurements. T.S. and F.C. performed conformational analysis of the glycopeptides in solution using NMR and molecular dynamics (MD) simulations and analyzed the conformational state of glycopeptides bound to SM3 using MD simulations. J.H.B., A.A., and F.C. carried out SPR analysis. Finally, R.G., J.A., R.F., and F.C. contributed to conceptualization, funding acquisition, investigation, methodology, resources, supervision, validation, and writing (original draft preparation, review, and editing). CRediT: **Ruslan Gibadullin** conceptualization, formal analysis, funding acquisition, investigation, supervision, writing - original draft, writing - review & editing; **Óscar Suárez** investigation, methodology; **Foivos Sokratis Lazaris** investigation, methodology; **Naiara Gutiez** investigation, methodology; **Estibaliz Atondo** investigation, methodology; **Sarai Araujo-Aris** investigation, methodology; **Ander Eguskiza** investigation, methodology; **Jiani Niu** investigation, methodology; **Ariel J. Kuhn** investigation, methodology; **Ana Sofia Grosso** formal analysis, investigation; **Héctor Rodriguez** formal analysis, investigation; **Fayna Garcia-Martin** data curation, formal analysis, investigation; **Filipa Marcelo** data curation, formal analysis, investigation; **Tanausú Santos** formal analysis, investigation; **Alberto Avenoza** data curation; **Jesús H Busto** data curation, formal analysis, funding acquisition, investigation, writing - review & editing; **Jesús M. Peregrina** data curation, formal analysis, investigation, writing - review & editing; **Samuel H. Gellman** supervision, writing - review & editing; **Juan Anguita** conceptualization, formal analysis, funding acquisition, investigation, supervision, writing - original draft, writing - review & editing; **Roberto Fiammengo** conceptualization, data curation, funding acquisition, investigation, supervision, writing - original draft, writing - review & editing; **Francisco Corzana** conceptualization, formal analysis, funding acquisition, investigation, supervision, writing - original draft, writing - review & editing.

Notes

The authors declare the following competing financial interest(s): S.H.G. is a co-founder of Longevity Biotech, Inc., which is pursuing biomedical applications of alpha/beta-peptides.

■ ACKNOWLEDGMENTS

This project has received partial funding from the European Union's Horizon 2020 research and innovation programme under the Marie Skłodowska-Curie grant agreement No. 956544. This work was also supported in part by the National Institutes of Health grant (R01 GM056414 and its successor R35 GM151985) awarded to S.H.G. We thank the *Agencia*

Estatal de Investigación (AEI, PID2021-127622OB-I00 to F.C., J.H.B. and O.S., PDC2022-133725-C21 to F.C, J.H.B., PID2020-120099RA-I00 to F.G.M., PID2021-124328OB-100 to J.A., and PRE-2019-091720 to S.A.), Universidad de La Rioja (REGI22/47 and REGI22/16) and *Asociación Española contra el Cáncer (AECC) sección La Rioja* (F.C. and J.M.P.). F.M. and A.S.G. acknowledge Fundação para a Ciência e Tecnologia Portugal (FCT-Portugal) for the MGL4Life project 10.54499/PTDC/QUI-OUT/2586/2020. F.M. thanks FCT-Portugal for CEECINST/00042/2021/CP1773/CT0011. F.M and A.S.G. thank UCIBIO project (UIDP/04378/2020 and UIDB/04378/2020), and Associate Laboratory Institute for Health and Bioeconomy - i4HB project (LA/P/0140/2020) and the National NMR Facility supported by FCT-Portugal (ROTEIRO/0031/2013−PINFRA/22161/2016, cofinanced by FEDER through COMPETE 2020, POCI and PORL and FCT through PIDDAC). T.S. thanks MCIN/AEI/10.13039/501100011033 and the European Union NextGenerationEU/PRTR for his *Juan de la Cierva* contract, JDC2022-048607-I. N.G. held a predoctoral grant from the Scientific Foundation of the Spanish Association Against Cancer in Bizkaia (PRDVZ222452GUTI). CICbioGUNE is the recipient of a Severo Ochoa Centro de Excelencia Award (CEX2021-001136-S). Supported in part by Fundación Jesús de Gangoiti. We are also grateful for partial support from the Vilas Trust and from the University of Wisconsin-Madison Office of the Vice Chancellor for Research and Graduate Education with funding from the Wisconsin Alumni Research Foundation. A.J.K. was supported in part by a postdoctoral fellowship from the National Institutes of Health (5F32AI176876).

REFERENCES

(1) Taylor-Papadimitriou, J.; Burchell, J. M.; Graham, R.; Beatson, R. Latest developments in MUC1 immunotherapy. *Biochem. Soc. Trans.* **2018**, *46*, 659−668.
(2) Apostolopoulos, V.; Stojanovska, L.; Gargosky, S. E. MUC1 (CD227): a multi-tasked molecule. *Cell. Mol. Life Sci.* **2015**, *72*, 4475−4500.
(3) Pinho, S. S.; Reis, C. A. Glycosylation in cancer: mechanisms and clinical implications. *Nat. Rev. Cancer* **2015**, *15*, 540−555.
(4) Kufe, D. W. Mucins in cancer: function, prognosis and therapy. *Nat. Rev. Cancer* **2009**, *9*, 874−885.
(5) Nath, S.; Mukherjee, P. MUC1: a multifaceted oncoprotein with a key role in cancer progression. *Trends Mol. Med.* **2014**, *20*, 332−342.
(6) Karsten, U. Binding patterns of DTR-specific antibodies reveal a glycosylation-conditioned tumor-specific epitope of the epithelial mucin (MUC1). *Glycobiology* **2004**, *14*, 681−692.
(7) Yoshimura, Y.; Denda-Nagai, K.; Takahashi, Y.; Nagashima, I.; Shimizu, H.; Kishimoto, T.; Noji, M.; Shichino, S.; Chiba, Y.; Irimura, T. Products of Chemoenzymatic Synthesis Representing MUC1 Tandem Repeat Unit with T-, ST- or STn-antigen Revealed Distinct Specificities of Anti-MUC1 Antibodies. *Sci. Rep.* **2019**, *9*, 16641.
(8) Coelho, H.; Matsushita, T.; Artigas, G.; Hinou, H.; Cañada, F. J.; Lo-Man, R.; Leclerc, C.; Cabrita, E. J.; Jiménez-Barbero, J.; Nishimura, S.-I.; et al. The Quest for Anticancer Vaccines: Deciphering the Fine-Epitope Specificity of Cancer-Related Monoclonal Antibodies by Combining Microarray Screening and Saturation Transfer Difference NMR. *J. Am. Chem. Soc.* **2015**, *137*, 12438−12441.
(9) Ju, T.; Otto, V. I.; Cummings, R. D. The Tn antigen-structural simplicity and biological complexity. *Angew. Chem., Int. Ed.* **2011**, *50*, 1770−1791.
(10) Blixt, O.; Bueti, D.; Burford, B.; Allen, D.; Julien, S.; Hollingsworth, M.; Gammerman, A.; Fentiman, I.; Taylor-Papadimitriou, J.; Burchell, J. M. Autoantibodies to aberrantly glycosylated MUC1 in early stage breast cancer are associated with a better prognosis. *Breast Cancer Res.* **2011**, *13*, R25.
(11) Wu, J.; Li, X.; Song, W.; Fang, Y.; Yu, L.; Liu, S.; Churilov, L. P.; Zhang, F. The roles and applications of autoantibodies in progression, diagnosis, treatment and prognosis of human malignant tumours. *Autoimmun. Rev.* **2017**, *16*, 1270−1281.
(12) Corzana, F.; Asín, A.; Eguskiza, A.; De Tomi, E.; Martín-Carnicero, A.; Martínez-Moral, M. P.; Mangini, V.; Papi, F.; Bretón, C.; Oroz, P.; et al. Detection of Tumor-Associated Autoantibodies in the Sera of Pancreatic Cancer Patients Using Engineered MUC1 Glycopeptide Nanoparticle Probes. *Angew. Chem., Int. Ed.* **2024**, *63*, No. e202407131.
(13) Cheever, M. A.; Allison, J. P.; Ferris, A. S.; Finn, O. J.; Hastings, B. M.; Hecht, T. T.; Mellman, I.; Prindiville, S. A.; Viner, J. L.; Weiner, L. M.; et al. The Prioritization of Cancer Antigens: A National Cancer Institute Pilot Project for the Acceleration of Translational Research. *Clin. Cancer Res.* **2009**, *15*, 5323−5337.
(14) Roy, R.; Mousavifar, L. Carrier diversity and chemical ligations in the toolbox for designing tumor-associated carbohydrate antigens (TACAs) as synthetic vaccine candidates. *Chem. Soc. Rev.* **2023**, *52*, 3353−3396.
(15) Wilson, R. M.; Danishefsky, S. J. A Vision for Vaccines Built from Fully Synthetic Tumor-Associated Antigens: From the Laboratory to the Clinic. *J. Am. Chem. Soc.* **2013**, *135*, 14462−14472.
(16) Gaidzik, N.; Westerlind, U.; Kunz, H. The development of synthetic antitumour vaccines from mucin glycopeptide antigens. *Chem. Soc. Rev.* **2013**, *42*, 4421−4442.
(17) Wolfert, M. A.; Boons, G. J. Adaptive immune activation: glycosylation does matter. *Nat. Chem. Biol.* **2013**, *9*, 776−784.
(18) Nativi, C.; Papi, F.; Roelens, S. Tn antigen analogues: the synthetic way to "upgrade" an attracting tumour associated carbohydrate antigen (TACA). *Chem. Commun.* **2019**, *55*, 7729−7736.
(19) Stergiou, N.; Urschbach, M.; Gabba, A.; Schmitt, E.; Kunz, H.; Besenius, P. The Development of Vaccines from Synthetic Tumor-Associated Mucin Glycopeptides and their Glycosylation-Dependent Immune Response. *Chem. Rec.* **2021**, *21*, 3313−3331.
(20) Feng, D.; Shaikh, A. S.; Wang, F. Recent Advance in Tumor-associated Carbohydrate Antigens (TACAs)-based Antitumor Vaccines. *ACS Chem. Biol.* **2016**, *11*, 850−863.
(21) Quoix, E.; Lena, H.; Losonczy, G.; Forget, F.; Chouaid, C.; Papai, Z.; Gervais, R.; Ottensmeier, C.; Szczesna, A.; Kazarnowicz, A.; et al. TG4010 immunotherapy and first-line chemotherapy for advanced non-small-cell lung cancer (TIME): results from the phase 2b part of a randomised, double-blind, placebo-controlled, phase 2b/3 trial. *Lancet Oncol.* **2016**, *17*, 212−223.
(22) Gao, T.; Cen, Q.; Lei, H. A review on development of MUC1-based cancer vaccine. *Biomed. Pharmacother.* **2020**, *132*, No. 110888.
(23) Schoen, R. E.; Boardman, L. A.; Cruz-Correa, M.; Bansal, A.; Kastenberg, D.; Hur, C.; Dzubinski, L.; Kaufman, S. F.; Rodriguez, L. M.; Richmond, E.; et al. Randomized, Double-Blind, Placebo-Controlled Trial of MUC1 Peptide Vaccine for Prevention of Recurrent Colorectal Adenoma. *Clin. Cancer Res.* **2023**, *29*, 1678−1688.
(24) Martinez-Saez, N.; Peregrina, J. M.; Corzana, F. Principles of mucin structure: implications for the rational design of cancer vaccines derived from MUC1-glycopeptides. *Chem. Soc. Rev.* **2017**, *46*, 7154−7175.
(25) Asín, A.; García-Martín, F.; Busto, H. J.; Avenoza, A.; Peregrina, M. J.; Corzana, F. Structure-based Design of Anti-cancer Vaccines: The Significance of Antigen Presentation to Boost the Immune Response. *Curr. Med. Chem.* **2022**, *29*, 1258−1270.
(26) Guerreiro, A.; Compañón, I.; Lazaris, F. S.; Labão-Almeida, C.; Oroz, P.; Ghirardello, M.; Marques, M. C.; Corzana, F.; Bernardes, G. J. L. Non-Natural MUC1 Glycopeptide Homogeneous Cancer Vaccine with Enhanced Immunogenicity and Therapeutic Activity. *Angew. Chem., Int. Ed.* **2024**, *63*, No. e202411009.
(27) Miles, J. J.; Tan, M. P.; Dolton, G.; Edwards, E. S. J.; Galloway, S. A. E.; Laugel, B.; Clement, M.; Makinde, J.; Ladell, K.; Matthews,

https://doi.org/10.1021/jacsau.5c00224
JACS Au 2025, 5, 2270−2284

K. K.; et al. Peptide mimic for influenza vaccination using nonnatural combinatorial chemistry. *J. Clin. Invest.* **2018**, *128*, 1569−1580.
(28) Wu, C. W.; Seurynck, S. L.; Lee, K. Y. C.; Barron, A. E. Helical Peptoid Mimics of Lung Surfactant Protein C. *Chem. Biol.* **2003**, *10*, 1057−1063.
(29) Chongsiriwatana, N. P.; Patch, J. A.; Czyzewski, A. M.; Dohm, M. T.; Ivankin, A.; Gidalevitz, D.; Zuckermann, R. N.; Barron, A. E. Peptoids that mimic the structure, function, and mechanism of helical antimicrobial peptides. *Proc. Natl. Acad. Sci. U.S.A.* **2008**, *105*, 2794−2799.
(30) Fremaux, J.; Venin, C.; Mauran, L.; Zimmer, R. H.; Guichard, G.; Goudreau, S. R. Peptide-oligourea hybrids analogue of GLP-1 with improved action in vivo. *Nat. Commun.* **2019**, *10*, 924.
(31) Gibadullin, R.; Morris, R. K.; Niu, J.; Sidney, J.; Sette, A.; Gellman, S. H. Thioamide Analogues of MHC I Antigen Peptides. *J. Am. Chem. Soc.* **2023**, *145*, 25559−25569.
(32) Horne, W. S.; Johnson, L. M.; Ketas, T. J.; Klasse, P. J.; Lu, M.; Moore, J. P.; Gellman, S. H. Structural and biological mimicry of protein surface recognition by α/β-peptide foldamers. *Proc. Natl. Acad. Sci. U.S.A.* **2009**, *106*, 14751−14756.
(33) Gibadullin, R.; Randall, C. J.; Sidney, J.; Sette, A.; Gellman, S. H. Backbone Modifications of HLA-A2-Restricted Antigens Induce Diverse Binding and T Cell Activation Outcomes. *J. Am. Chem. Soc.* **2021**, *143*, 6470−6481.
(34) Cheloha, R. W.; Chen, B.; Kumar, N. N.; Watanabe, T.; Thorne, R. G.; Li, L.; Gardella, T. J.; Gellman, S. H. Development of Potent, Protease-Resistant Agonists of the Parathyroid Hormone Receptor with Broad β Residue Distribution. *J. Med. Chem.* **2017**, *60*, 8816−8833.
(35) Seebach, D.; Gardiner, J. β-Peptidic Peptidomimetics. *Acc. Chem. Res.* **2008**, *41*, 1366−1375.
(36) Cheloha, R. W.; Woodham, A. W.; Bousbaine, D.; Wang, T.; Liu, S.; Sidney, J.; Sette, A.; Gellman, S. H.; Ploegh, H. L. Recognition of Class II MHC Peptide Ligands That Contain β-Amino Acids. *J. Immunol.* **2019**, *203*, 1619−1628.
(37) Kaszowska, M.; Norgren, A. S.; Arvidson, P. I.; Sandström, C. Studies on the interactions between glycosylated β3-peptides and the lectin Vicia villosa by saturation transfer difference NMR spectroscopy. *Carbohydr. Res.* **2009**, *344*, 2577−2580.
(38) Norgren, A. S.; Geitmann, M.; Danielson, U. H.; Arvidsson, P. I. Biomolecular recognition of glycosylated β3-peptides by GalNAc specific lectins. *J. Mol. Recognit.* **2007**, *20*, 132−138.
(39) Johnson, L. M.; Gellman, S. H. Chapter Nineteen - α-Helix Mimicry with α/β-Peptides. In *Methods in Enzymology*; Keating, A. E., Ed.; Academic Press, 2013; Vol. *523*, pp 407−429.
(40) Checco, J. W.; Lee, E. F.; Evangelista, M.; Sleebs, N. J.; Rogers, K.; Pettikiriarachchi, A.; Kershaw, N. J.; Eddinger, G. A.; Belair, D. G.; Wilson, J. L.; et al. α/β-Peptide Foldamers Targeting Intracellular Protein−Protein Interactions with Activity in Living Cells. *J. Am. Chem. Soc.* **2015**, *137*, 11365−11375.
(41) Cheloha, R. W.; Maeda, A.; Dean, T.; Gardella, T. J.; Gellman, S. H. Backbone modification of a polypeptide drug alters duration of action in vivo. *Nat. Biotechnol.* **2014**, *32*, 653−655.
(42) Dokurno, P.; Bates, P. A.; Band, H. A.; Stewart, L. M.; Lally, J. M.; Burchell, J. M.; Taylor-Papadimitriou, J.; Snary, D.; Sternberg, M. J.; Freemont, P. S. Crystal structure at 1.95 A resolution of the breast tumour-specific antibody SM3 complexed with its peptide epitope reveals novel hypervariable loop recognition. *J. Mol. Biol.* **1998**, *284*, 713−728.
(43) Bermejo, I. A.; Guerreiro, A.; Eguskiza, A.; Martínez-Sáez, N.; Lazaris, F. S.; Asín, A.; Somovilla, V. J.; Compañón, I.; Raju, T. K.; Tadic, S.; et al. Structure-Guided Approach for the Development of MUC1-Glycopeptide-Based Cancer Vaccines with Predictable Responses. *JACS Au* **2024**, *4*, 150−163.
(44) Companon, I.; Guerreiro, A.; Mangini, V.; Castro-Lopez, J.; Escudero-Casao, M.; Avenoza, A.; Busto, J. H.; Castillon, S.; Jimenez-Barbero, J.; Asensio, J. L.; et al. Structure-Based Design of Potent Tumor-Associated Antigens: Modulation of Peptide Presentation by Single-Atom O/S or O/Se Substitutions at the Glycosidic Linkage. *J. Am. Chem. Soc.* **2019**, *141*, 4063−4072.
(45) Martinez-Saez, N.; Castro-Lopez, J.; Valero-Gonzalez, J.; Madariaga, D.; Companon, I.; Somovilla, V. J.; Salvado, M.; Asensio, J. L.; Jimenez-Barbero, J.; Avenoza, A.; et al. Deciphering the Non-Equivalence of Serine and Threonine O-Glycosylation Points: Implications for Molecular Recognition of the Tn Antigen by an anti-MUC1 Antibody. *Angew. Chem., Int. Ed.* **2015**, *54*, 9830−9834.
(46) Movahedin, M.; Brooks, T. M.; Supekar, N. T.; Gokanapudi, N.; Boons, G.-J.; Brooks, C. L. Glycosylation of MUC1 influences the binding of a therapeutic antibody by altering the conformational equilibrium of the antigen. *Glycobiology* **2017**, *27*, 677−687.
(47) Fontenot, J. D.; Tjandra, N.; Bu, D.; Ho, C.; Montelaro, R. C.; Finn, O. J. Biophysical Characterization of One-, Two-, and Three-Tandem Repeats of Human Mucin (muc-1) Protein Core1. *Cancer Res.* **1993**, *53*, 5386−5394.
(48) Stapley, B. J.; Creamer, T. P. A survey of left-handed polyproline II helices. *Protein Sci.* **1999**, *8*, 587−595.
(49) Corzana, F.; Busto, J. H.; Jiménez-Osés, G.; García De Luis, M.; Asensio, J. L.; Jiménez-Barbero, J.; Peregrina, J. M.; Avenoza, A. Serine versus Threonine Glycosylation: The Methyl Group Causes a Drastic Alteration on the Carbohydrate Orientation and on the Surrounding Water Shell. *J. Am. Chem. Soc.* **2007**, *129*, 9458−9467.
(50) Ebeling, W.; Hennrich, N.; Klockow, M.; Metz, H.; Orth, H. D.; Lang, H. Proteinase K from Tritirachium album Limber. *Eur. J. Biochem.* **1974**, *47*, 91−97.
(51) Maraming, P.; Daduang, J.; Kah, J. C. Y. Conjugation with gold nanoparticles improves the stability of the KT2 peptide and maintains its anticancer properties. *RSC Adv.* **2021**, *12*, 319−325.
(52) Kalimuthu, K.; Lubin, B.-C.; Bazylevich, A.; Gellerman, G.; Shpilberg, O.; Luboshits, G.; Firer, M. A. Gold nanoparticles stabilize peptide-drug-conjugates for sustained targeted drug delivery to cancer cells. *J. Nanobiotechnol.* **2018**, *16*, 34.
(53) Qu, J.; Yu, H.; Li, F.; Zhang, C.; Trad, A.; Brooks, C.; Zhang, B.; Gong, T.; Guo, Z.; Li, Y.; et al. Molecular basis of antibody binding to mucin glycopeptides in lung cancer. *Int. J. Oncol.* **2016**, *48*, 587−594.
(54) Lee, A. V.; Oesterreich, S.; Davidson, N. E. MCF-7 cells−changing the course of breast cancer research and care for 45 years. *J. Natl. Cancer Inst.* **2015**, *107*, djv073.
(55) Vermeulen, S. J.; Chen, T. R.; Speleman, F.; Nollet, F.; Van Roy, F. M.; Mareel, M. M. Did the four human cancer cell lines DLD-1, HCT-15, HCT-8, and HRT-18 originate from one and the same patient? *Cancer Genet. Cytogenet.* **1998**, *107*, 76−79.
(56) Tan, E.; Chin, C. S. H.; Lim, Z. F. S.; Ng, S. K. HEK293 Cell Line as a Platform to Produce Recombinant Proteins and Viral Vectors. *Front. Bioeng. Biotechnol.* **2021**, *9*, No. 796991.
(57) Ivashkiv, L. B. IFNγ: signalling, epigenetics and roles in immunity, metabolism, disease and cancer immunotherapy. *Nat. Rev. Immunol.* **2018**, *18*, 545−558.
(58) Cheloha, R. W.; Sullivan, J. A.; Wang, T.; Sand, J. M.; Sidney, J.; Sette, A.; Cook, M. E.; Suresh, M.; Gellman, S. H. Consequences of Periodic α-to-β3 Residue Replacement for Immunological Recognition of Peptide Epitopes. *ACS Chem. Biol.* **2015**, *10*, 844−854.
(59) Guichard, G.; Zerbib, A.; Le Gal, F.-A.; Hoebeke, J.; Connan, F.; Choppin, J.; Briand, J.-P.; Guillet, J.-G. Melanoma Peptide MART-1(27−35) Analogues with Enhanced Binding Capacity to the Human Class I Histocompatibility Molecule HLA-A2 by Introduction of a β-Amino Acid Residue: Implications for Recognition by Tumor-Infiltrating Lymphocytes. *J. Med. Chem.* **2000**, *43*, 3803−3808.
(60) Reinelt, S.; Marti, M.; Dédier, S.; Reitinger, T.; Folkers, G.; de Castro, J. A. L.; Rognan, D. Beta-amino Acid Scan of a Class I Major Histocompatibility Complex-restricted Alloreactive T-cell Epitope *. *J. Biol. Chem.* **2001**, *276*, 24525−24530.
(61) Webb, A. I.; Dunstone, M. A.; Williamson, N. A.; Price, J. D.; de Kauwe, A.; Chen, W.; Oakley, A.; Perlmutter, P.; McCluskey, J.; Aguilar, M.-I.; et al. T Cell Determinants Incorporating β-Amino Acid

https://doi.org/10.1021/jacsau.5c00224
JACS Au 2025, 5, 2270−2284

Residues Are Protease Resistant and Remain Immunogenic In Vivo1. *J. Immunol.* **2005**, *175*, 3810−3818.
(62) Cheng, R. P.; Gellman, S. H.; DeGrado, W. F. beta-Peptides: from structure to function. *Chem. Rev.* **2001**, *101*, 3219−3232.
(63) Cabrele, C.; Martinek, T. A.; Reiser, O.; Berlicki, Ł. Peptides Containing *β*-Amino Acid Patterns: Challenges and Successes in Medicinal Chemistry. *J. Med. Chem.* **2014**, *57*, 9718−9739.
(64) Bermejo, I. A.; Navo, C. D.; Castro-López, J.; Guerreiro, A.; Jiménez-Moreno, E.; Sánchez Fernández, E. M.; García-Martín, F.; Hinou, H.; Nishimura, S.-I.; García Fernández, J. M.; et al. Synthesis, conformational analysis and in vivo assays of an anti-cancer vaccine that features an unnatural antigen based on an sp2-iminosugar fragment. *Chem. Sci.* **2020**, *11*, 3996−4006.
(65) Plattner, C.; Höfener, M.; Sewald, N. One-Pot Azidochlorination of Glycals. *Org. Lett.* **2011**, *13*, 545−547.
(66) Keller, R. *The Computer Aided Resonance Assignment Tutorial*; Cantina Verlag, 2004.
(67) Case, D. A.; Belfon, K.; Ben-Shalom, I. Y.; Brozell, S. R.; Cerutti, D. S.; Cheatham, III, T. E.; Cruzeiro, V. W. D.; Darden, T. A.; Duke, R. E.; Giambasu, G.; Gilson, M. K.; Gohlke, H.; Goetz, A. W.; Harris, R.; Izadi, S.; Izmailov, S. A.; Kasavajhala, K.; Kovalenko, A.; Krasny, R.; Kurtzman, T.; Lee, T. S.; LeGrand, S.; Li, P.; Lin, C.; Liu, J.; Luchko, T.; Luo, R.; Man, V.; Merz, K. M.; Miao, Y.; Mikhailovskii, O.; Monard, G.; Nguyen, H.; Onufriev, A.; Pan, F.; Pantano, S.; Qi, R.; Roe, D. R.; Roitberg, A.; Sagui, C.; Schott-Verdugo, S.; Shen, J.; Simmerling, C. L.; Skrynnikov, N. R.; Smith, J.; Swails, J.; Walker, R. C.; Wang, J.; Wilson, L.; Wolf, R. M.; Wu, X.; Xiong, Y.; Xue, Y.; York, D. M.; Kollman, P. A. *AMBER 2020*; University of California: San Francisco, 2020.
(68) Maier, J. A.; Martinez, C.; Kasavajhala, K.; Wickstrom, L.; Hauser, K. E.; Simmerling, C. ff14SB: Improving the Accuracy of Protein Side Chain and Backbone Parameters from ff99SB. *J. Chem. Theory Comput.* **2015**, *11*, 3696−3713.
(69) Wang, J.; Wolf, R. M.; Caldwell, J. W.; Kollman, P. A.; Case, D. A. Development and testing of a general amber force field. *J. Comput. Chem.* **2004**, *25*, 1157−1174.
(70) Kirschner, K. N.; Yongye, A. B.; Tschampel, S. M.; González-Outeiriño, J.; Daniels, C. R.; Foley, B. L.; Woods, R. J. GLYCAM06: a generalizable biomolecular force field. *Carbohydrates. J. Comput. Chem.* **2008**, *29*, 622−655.
(71) Jakalian, A.; Jack, D. B.; Bayly, C. I. Fast, efficient generation of high-quality atomic charges. AM1-BCC model: II. Parameterization and validation. *J. Comput. Chem.* **2002**, *23*, 1623−1641.
(72) Jorgensen, W. L.; Chandrasekhar, J.; Madura, J. D.; Impey, R. W.; Klein, M. L. Comparison of simple potential functions for simulating liquid water. *J. Chem. Phys.* **1983**, *79*, 926−935.
(73) Darden, T.; York, D.; Pedersen, L. Particle mesh Ewald: An N·log(N) method for Ewald sums in large systems. *J. Chem. Phys.* **1993**, *98*, 10089−10092.
(74) Grabar, K. C.; Freeman, R. G.; Hommer, M. B.; Natan, M. J. Preparation and Characterization of Au Colloid Monolayers. *Anal. Chem.* **1995**, *67*, 735−743.
(75) Brody, J. R.; Kern, S. E. Sodium boric acid: a Tris-free, cooler conductive medium for DNA electrophoresis. *Biotechniques* **2004**, *36*, 214−216.

https://doi.org/10.1021/jacsau.5c00224
JACS Au 2025, 5, 2270−2284